N-cadherin directs the collective Schwann cell migration required for nerve regeneration through Slit2/3 mediated contact inhibition of locomotion

Julian J.A Hoving[1], Elizabeth Harford-Wright[1], Patrick Wingfield-Digby[1], Anne-Laure Cattin[1], Mariana Campana[1], Alex Power[1], Toby Morgan[1], Erica Torchiaro[1], Victor Quereda[1], and Alison C. Lloyd[1,2]

[1]UCL Laboratory for Molecular Cell Biology and the UCL Cancer Institute, University College London, Gower Street, WC1E 6BT

Tel +44 (0)207 679 2240

[2]Corresponding author: alison.lloyd@ucl.ac.uk

Abstract

Collective cell migration is fundamental for the development of organisms and in the adult, for tissue regeneration and in pathological conditions such as cancer. Migration as a coherent group requires the maintenance of cell-cell interactions, while contact inhibition of locomotion (CIL), a local repulsive force, can propel the group forward. Here we show that the cell-cell interaction molecule, N-cadherin, regulates both adhesion and repulsion processes during rat Schwann cell (SC) collective migration, which is required for peripheral nerve regeneration. However, distinct from its role in cell-cell adhesion, the repulsion process is independent of N-cadherin trans-homodimerisation and the associated adherens junction complex. Rather, the extracellular domain of N-cadherin is required to present the repulsive Slit2/Slit3 signal at the cell-surface. Inhibiting Slit2/Slit3 signalling inhibits CIL and subsequently collective Schwann cell migration, resulting in adherent, nonmigratory cell clusters. Moreover, analysis of ex vivo explants from mice following sciatic nerve injury showed that inhibition of Slit2 decreased Schwann cell collective migration and increased clustering of Schwann cells within the nerve bridge. These findings provide insight into how opposing signals can mediate collective cell migration and how CIL pathways are promising targets for inhibiting pathological cell migration.

Impact Statement

N-cadherin and Slit2/3/Robo interactions provide the outward force to drive collective Schwann cell migration during nerve regeneration, identifying a dual role for N-cadherin in both adhesion and repulsion processes during Schwann cell collective migration.

Introduction

Tissue and organ morphogenesis requires the orchestration of the movement of large numbers of cells (Klambt, 2009; Scarpa & Mayor, 2016). In the adult, cell migration is less frequent but is important for aspects of tissue renewal and immune surveillance and can be activated following an injury to contribute to wound healing and tissue regeneration (Friedl & Gilmour, 2009; Moreau et al., 2018; Shaw & Martin, 2016; Worbs et al., 2017). Moreover, these modes of migration are frequently recapitulated during pathologies such as cancer, allowing tumour cells to spread from their original site (Friedl & Gilmour, 2009; Madsen & Sahai, 2010; Reymond et al., 2013).

Peripheral nerve is one of the few tissues in the mammalian adult that retains the ability to regenerate following an injury (Jessen et al., 2015; Poss, 2010; Zochodne, 2012). We have previously shown that the successful regeneration of a transected nerve requires the collective migration of cords of Schwann cells (SCs) that transport re-growing axons across the injury site (Parrinello et al., 2010; Stierli et al., 2019; Stierli et al., 2018). Moreover, SC cords gain directionality across the wound by migrating along a newly formed polarised vasculature, which develops prior to SC migration (Cattin et al., 2015; Cattin & Lloyd, 2016). However, it has become clear that the collective migration of SCs as cords is an adaptive process, as SCs cultured alone exhibit contact inhibition of locomotion (CIL) (Parrinello et al., 2010), a process in which two cells repulse each other upon contact resulting in the separation of cells (Abercrombie & Heaysman, 1953, 1954; Carmona-Fontaine et al., 2008; Davis et al., 2015). Following an injury however, SC collective migration is triggered following interactions with fibroblasts that come into contact with SCs as they enter the wound-site (Parrinello et al., 2010). This heterotypic interaction with fibroblasts transforms SC behaviour from repulsive to attractive, a process mediated by ephrinB/EphB2signalling inducing a Sox2-mediated re-localisation of N-cadherin to the site of cell-cell junctions, that results in SCs migrating as cellular cords (Parrinello et al., 2010).

Recently, CIL has been shown to play a role in the dispersal of cells during development, with CIL promoting the spread of cells through tissues (Davis et al., 2012; Villar-Cervino et al., 2013). Moreover, CIL is also important for providing an outward force during collective cell migration, in

that, CIL regulates the polarisation of cells, by inhibiting local protrusions at the site of cell-cell contact and inducing protrusion formation at the free edge, thus promoting outward migration (Abercrombie & Heaysman, 1953, 1954; Carmona-Fontaine et al., 2008; Davis et al., 2015; Scarpa et al., 2015; Theveneau et al., 2010). This implies that collective migration requires the maintenance of a CIL signal in the presence of a stronger adhesive signal, but how this can be achieved is poorly understood.

Here we show that N-cadherin mediates both the adhesive and repulsive forces required for collective SC migration but via two distinct mechanisms; with adhesion dependent on the Sox2-stabilised, N-cadherin adherens-junction complex, while repulsion is the result of N-cadherin presenting a Slit2 and Slit3 repulsive signal. Moreover, because of this dual role, inhibiting the CIL signal results in the formation of tight clusters of non-migratory cells. Consistent with this, in ex vivo slices from mice that had undergone sciatic nerve injury, inhibition of the Slit2 repulsive signal impaired collective SC migration resulting in cell clusters that appeared to lack directionality. The ability of N-cadherin to simultaneously regulate adhesion and CIL shows how these opposing processes can be coordinated to achieve outward collective migration and that CIL signals may present an attractive target for inhibiting unwanted collective cell migration.

Results

N-cadherin is required for contact inhibition of locomotion between Schwann cells

We previously showed that EphB2 activation of Sox2 results in the clustering of SCs, but video analysis indicated that these clustered cells maintain CIL, as the cells appeared to be repulsing each other within the cluster (Parrinello et al., 2010). This is consistent with the migration of SC cords during nerve regeneration, which would be predicted to require a force, such as CIL, to drive migration forward (Carmona-Fontaine et al., 2008; Haeger et al., 2015; Roycroft et al., 2018; Theveneau et al., 2010). N-cadherin has been implicated in CIL in other cell types (Scarpa et al., 2015; Tanaka et al., 2012; Theveneau et al., 2010), so we addressed whether N-cadherin was also required for the regulation of SC collective migration. To do this, we initially blocked N-cadherin

expression using two independent siRNAs (Figure 1-figure supplement 1a-b) and performed a scratch assay (Figure 1a-e). Time-lapse microscopy showed that while scrambled control siRNA-treated cells migrated in a directional manner to efficiently close the gap, N-cadherin-knockdown cells closed the gap more slowly, as they migrated in multiple directions, over each other and with a lack of persistent migration towards the gap (Figure 1a-d). This difference was not due to a defect in migration speed, as individual N-cadherin-knockdown cells migrated more rapidly (Figure 1e), suggesting that N-cadherin was required for the cell-contact dependent process driving outward migration. Consistent with this, confluent control SCs form a monolayer and stable junctions, whereas N-cadherin knockdown cells were unable to form junctions and grew on top of each other (Figure 1a and Figure 1-figure supplement 1b-c). This indicated N-cadherin knockdown cells had lost the ability to recognise each other, and that the loss of contact-dependent outward migration observed in the collective migration assay may be due to loss of CIL.

To study the role of N-cadherin in homotypic CIL between SCs, we assessed CIL upon cell-cell contact of SCs cultured at low density. To quantify this, we looked at single cell interactions and determined three different responses of the protrusions after the initial contact was made: Retraction, SCs retract their protrusions and change direction of migration; No retraction; SCs interact for longer than 5 hours and do not change their direction or migrate away following contact; Overlapping, SCs continue to migrate following contact with their protrusions or cells bodies migrating on top of each other.

Live-imaging of siRNA scrambled control SCs, showed that SCs migrate in multiple directions, making frequent, seemingly random, protrusions and retractions in multiple directions. However, upon contact with another SC, the SC nearly always retracts the contacting protrusion, appears repulsed, and changes its direction of migration (Figure 1-Video 1, Figure 1f, quantified in Figure 1g), behaviours that are features of CIL (Abercrombie & Heaysman, 1953, 1954) and is consistent with what we observed previously (Parrinello et al., 2010). In contrast, while free-moving N-cadherin knockdown cells continued to make random protrusions and frequently change direction, upon contact they behaved very differently to control cells, in that they continued to move forward

upon contact and migrated on top of each other, a behaviour we termed overlapping. We did still observe retractions in the N-cadherin knock-down cells, however, we interpret this as background behaviour of cells that frequently change direction, even in the absence of contact. In contrast, the overlapping behaviour was rarely seen in control cells, showing that N-cadherin knockdown cells show no apparent recognition of each other and no CIL.

To confirm these results, we performed an additional quantification, which determines whether a cell changes its direction of movement following contact, compared to free moving cells (Paddock & Dunn, 1986). In control cells, a significant difference between the displacement of free moving and cells in contact was observed (Figure 1h), as control cells change direction after contact. In contrast, in N-cadherin knockdown cells, no difference was observed between free moving and colliding cells, indicating that the cellular repulsion signal has been lost in these cells (Figure 1h). These results show that in addition to mediating adhesion between SCs, N-cadherin is also required for CIL between collectively migrating SCs.

N-cadherin dependent CIL is independent of the adherens junction complex

To understand how N-cadherin can mediate both cell:cell adhesion and CIL, we addressed whether both processes act via the N-cadherin adherens complex, which has previously been implicated in both processes (Parrinello et al., 2010; Scarpa et al., 2015; Theveneau et al., 2010). N-cadherin transmits adhesive forces between neighbouring cells by forming trans-homodimers which relay signalling via the well characterised intracellular adherens complex to the actin cytoskeleton (Brasch et al., 2012; Harris & Tepass, 2010; Peglion & Etienne-Manneville, 2013; Peglion et al., 2014). We initially used time-lapse microscopy to analyse CIL between red-labelled, control-treated cells and green-labelled, N-cadherin knockdown cells in cocultures to determine the requirement for N-cadherin homodimers between the cells (Figure 2a, Figure 2-Video 1). Surprisingly, while a N-cadherin knockdown cell (N2) invaded another N-cadherin knockdown cell (N1), the same cell was repulsed upon subsequent contact with a control cell (C2) (Figure 2a, Quantified in Figure 2b). This suggested that N-cadherin is required to present a repulsion signal and induce repulsion but is not required for a cell to be repulsed. Consistent with this, when

analysing the response of the siRNA scrambled control cells (C2) upon contact with an N-cadherin knockdown cell (N2), the majority of the control cells were not repulsed (Figure 2a, quantified in 2b). However, the control cells did not invade the N-cadherin knockdown cells, as the N-cadherin knockdown cells were repulsed and migrated away (Figure 2-Video 1, Figure 2b). This shows that N-cadherin is required to present a repulsion signal and induce repulsion, but not to be repulsed (Video 2, Figure 2c).

To further test this observation, we performed a dual chamber assay, which assessed the ability of cells to form a boundary upon the closure of a gap. Consistent with the single-cell analysis, we found that whereas control cells formed a boundary upon gap closure and N-cadherin knockdown cells migrated on top of each other, N-cadherin knockdown cells were repulsed by the approaching control-treated cells and were unable to invade (Figure 2d and Supplementary Figure 2a). These results confirmed that N-cadherin is only required to present the repulsive CIL signal, but not to be repulsed. Moreover, it suggests that N-cadherin mediates CIL independent of trans-homodimerisation, implying a distinct mechanism mediates CIL.

While the repulsion signal is independent of the trans-homodimerisation of N-cadherin, it remained a possibility that the proteins associated with the classical N-cadherin-adherens complex were required for the CIL signal. We therefore tested whether α-catenin and p120-catenin, which are known to physically connect N-cadherin to the actin cytoskeleton and regulate the stability of the N-cadherin adherens complex, are required for CIL (Buckley et al., 2014; Peglion & Etienne-Manneville, 2013; Peglion et al., 2014; Pokutta & Weis, 2000; Rimm et al., 1995; Yao et al., 2014). Time-lapse microscopy showed that efficient knockdown of α-catenin in SCs had no effect on CIL, as the cells still repulsed each other despite an increase in cell velocity (Figure 2e-f and Figure 2-figure supplement 1b-c). However, consistent with previous reports, the connection of N-cadherin to the actin cytoskeleton appeared to be disrupted, as shown by the more cortical appearance of the actin cytoskeleton at N-cadherin cell-cell contacts (Figure 2-figure supplement 1b). Similarly, SCs depleted of p120 catenin still repulsed each other upon contact, although there was a slight but significant decrease in repulsive events in cells treated with siRNA2 (Figure 2g-h

and Figure 2-figure supplement1d-e). Consistent with the role of p120-catenin in regulating cadherin levels at the cell-surface (Davis et al., 2003; Miyashita & Ozawa, 2007; Nanes et al., 2012; Peglion & Etienne-Manneville, 2013), we found a strong decrease in the levels of N-cadherin at the cell surface, although this was still concentrated at cell:cell contacts. However, this was greater in cells treated with the more efficient siRNA2, making it likely that a decrease in N-cadherin at the cell-surface was responsible for the small effect on CIL (Figure 2g-h andFigure 2-figure supplement 1d-e). Together these results indicated that N-cadherin mediated CIL is both independent of trans-homodimerisation and acts independently of the adherens junction complex.

The extracellular domain of N-cadherin is sufficient to mediate CIL

To investigate how N-cadherin mediates CIL, we tested which domains of N-cadherin were sufficient to rescue CIL in N-cadherin knocked-down cells. Western blotting showed that either full length siRNA-resistant, tomato-tagged N-cadherin or mutants lacking the intracellular domain or the extracellular domain were expressed at similar levels (Figure 3a-b) (Shih & Yamada, 2012). Confocal images showed that in SCs expressing the full-length exogenous N-cadherin construct, N-cadherin was localised at cell-cell junctions, and co-localised with α-catenin and p120-catenin (Figure 3-figure supplement 1). In contrast, in SCs expressing the intracellular domain of N-cadherin, N-cadherin did not form junctions and was observed at the membrane, co-localised with α-catenin and p120 catenin (Figure 3-figure supplement 1). Whereas in cells expressing the extracellular domain of N-cadherin, N-cadherin was present at the cell-cell junctions but was unable to recruit α-catenin and p120-catenin (Figure 3-figure supplement 1).

To analyse the effect of these constructs on CIL, we quantified the response of N-cadherin knockdown cells upon contact with N-cadherin construct-expressing cells at low density. Consistent with our earlier results, N-cadherin knockdown cells were repulsed by an N-cadherin expressing cell. As expected, while N-cadherin knockdown cells migrated over each other, they were repulsed upon contact with cells rescued with full-length N-cadherin (Figure 3-Video 1 and Figure 3c, quantified in Figure 3d), confirming that loss of CIL is specific to N-cadherin. In contrast, CIL was not rescued by SCs expressing the intracellular domain of N-cadherin (Figure

3c-d). Strikingly, CIL was fully rescued by SCs expressing the extracellular domain of N-cadherin showing that intracellular signalling by N-cadherin is not required to mediate CIL (Figure 3c-d). This result is consistent with our findings that the adherens junction complex is not required for N-cadherin mediated CIL, and together with our findings that N-cadherin is only required to present a repulsion signal, suggests that an additional co-repulsion signal may be required to mediate CIL in SCs.

Glypican-4 and Slit2/Slit3 are required for CIL

We have previously shown that SCs are repulsed by fibroblasts in an ephrinB/EphB2-dependent manner (Parrinello et al., 2010), which induces cell clustering via activation of Sox2-dependent re-localisation of N-cadherin to cell-cell junctions. We thus reasoned that ephrinB/EphB2 was unlikely to be responsible for the homotypic CIL between SCs and this was confirmed in knockdown experiments (Supplementary Fig 4a).

To identify the homotypic CIL signal, we performed a series of proteomic screens, using N-cadherin or the extracellular domain of N-cadherin as bait, followed by co-immunoprecipitation and qualitative Mass Spectrometry analysis. In these analyses, peptides of Glypican-4, a Glycosylphosphatidylinositol (GPI)-linked heparan sulfate proteoglycan, were detected in N-cadherin pull-down samples. Glypicans have previously been shown to play a role in axonal guidance and collective cell migration, so although not previously implicated in CIL, Glypican-4 was an interesting candidate (Blanchette et al., 2015; Johnson et al., 2004; Venero Galanternik et al., 2015). To test if Glypican-4 was required for mediating repulsive signals between SCs, we knocked down Glypican-4 (Figure 4-figure supplement 1b) and performed a CIL assay. Intriguingly, Glypican-4 knockdown cells did not repulse upon contact, nor did they invade (Figure 4a). Instead, upon contact it appeared that the cells adhered to each other and formed clusters (Figure 4b-c, Figure 4-Video 1), with cell velocity prior to cluster formation unaffected (Figure 4-figure supplement 1c). This result was in stark contrast to N-cadherin knockdown cells, which migrated over the top of each other upon contact (Figure 1 f-g). Moreover, the cell clusters appeared to behave differently to the clusters resulting from Sox-2 over-expression, with repulsive

forces not evident between Glypican-4 knockdown cells upon contact, resulting in “quieter” clusters that were no longer polarised towards outward migration **(**Figure 4c, Figure 4-Video 1 and Video 2**)**. Consistent with this finding, N-cadherin was still present at the membrane in Glypican-4 knockdown cells with confocal images showing that N-cadherin accumulated at the cell-cell contacts, forming longer junctions compared to the control (Figure 4c). This suggested that Glypican-4 is involved in the N-cadherin-dependent CIL signal and that in its absence SCs form more stable homotypic junctions, resulting in quieter clusters of cells. Consistent with this hypothesis, double knockdown of both Glypican-4 and N-cadherin, resulted in cells that grew on top of each other, mimicking the N-cadherin knockdown phenotype (Figure 4figure supplement 1d-e), highlighting the key role for N-cadherin in mediating the repulsive signal that is independent of its role at the cell:cell junctions.

Glypicans are GPI-linked proteins that have been reported to act as co-receptors in several signalling pathways including Slit/Robo, Wnt, FGF, Hedgehog, and Bone Morphogenetic pathways or can modulate the accessibility of ligands. However, they are not thought to act as ligands themselves, indicating another signal may be required (Sarrazin et al., 2011; Ypsilanti et al., 2010). Of particular interest were the Slit/Robo signalling pathways, whose repulsive signals are known to play a role in axonal guidance (Brose et al., 1999; Jia et al., 2005; Kaneko et al., 2010; Kidd et al., 1999; Nguyen-Ba-Charvet et al., 2004; Ypsilanti et al., 2010). Previous studies have shown that of the three Slit genes, Slit2 and Slit3 are predominately expressed by SCs (Carr et al., 2017; Chen et al., 2020; Wang et al., 2013). We first confirmed this finding (Figure 4-figure supplement 1f) and then performed knockdowns of both Slit2 and Slit3 in SCs (Figure 4-figure supplement 1g) and performed CIL assays. Initial studies showed a small loss of CIL with individual siRNA, but the phenotype was not as strong as seen with Glypican-4, possibly because of compensation between the two molecules (data not shown). We therefore performed a double knockdown of Slit2 and Slit3Figure and found that Slit2/Slit3 knockdown cells behaved similarly to Glypican-4 cells in that they no longer repulsed upon contact, showing instead, increased levels

of adhesion (Figure 4d, Figure 4-Video 2) resulting in the formation of cell clusters with increased N-cadherin-mediated junctions compared to the control (Figure 4e-f) .

To induce signalling, Slits can bind to Roundabout (Robo) receptors (Ronca et al., 2001; Zhang et al., 2004), which have been shown to mediate Slit-repulsive signals during neuronal development. Expression analysis showed that SCs express Robo 1,2 and 4 (Figure 4-figure supplement 1f), consistent with previous findings that Robo1 is expressed by SCs (Carr et al., 2017). To determine whether Slit acts via the Robo receptors, we performed knockdown experiments for Robo1 and Robo2 in SCs (Figure 4-figure supplement 1h) and assessed their ability to form clusters. Similarly, to the Slit2/3 KDs, loss of either the Robo1 or Robo2 receptor in SCs resulted in a strong increase in cluster formation (Figure 4g-h), that resembled the quieter, round clusters observed with Slit2/3 and Glypican-4 KDs. Together these results indicate that Slit2/3 mediates the CIL signal through interactions with Robo1/2 and Glypican-4.

Following nerve injury, we have previously shown that SCs migrate collectively in polarised cords via activation of Sox2 and the resulting stabilisation of N-cadherin at the cell-cell junctions (Cattin et al., 2015; Parrinello et al., 2010). To compare the difference between these migratory SC clusters and the clusters induced by loss of Slit2/Slit3, we overexpressed Sox2 in SCs and compared them to Slit2/Slit3 KD SCs. Overexpression of Sox2 resulted in polarised clusters of SCs with increased N-cadherin at the cell-cell contacts (Figure 4i). In contrast, the clusters associated with Slit2/Slit3 knockdown had a very different morphology, consisting of more "rounded" SCs, which lacked polarity, suggesting that the absence of Slit2/Slit3 signals between the cells results in cell clusters that lack an outward force to drive collective migration (Figure 4i, quantified in Figure 4-figure supplement 1i, and Figure 4-Video 2).

Loss of N-cadherin alters Slit2/Slit3 localisation at the cell surface

We have shown that both N-cadherin and Slit2/Slit3 are required for CIL between SCs. We hypothesised that this could be due to the loss of the repulsive Slit2/Slit3 signal in cells lacking N-cadherin. However, following N-cadherin knockdown, little change was detected in total Slit2 and Slit3 protein levels (Figure 5-figure supplement 1a) and mRNA levels of Slit2/3 and Glypican 4

were also not affected (Figure 5-figure supplement 1b) indicating a post-translational mechanism was involved. Co-immunoprecipitation experiments showed that Slit2 could be pulled down by N-cadherin (Figure 5c) and live-imaging of SCs expressing tagged N-cadherin revealed that N-cadherin is a highly dynamic protein arriving in waves towards the cell's moving front, suggesting that perhaps a pool of N-cadherin was interacting with Slit2/Slit3 to facilitate its transport to the cell-surface to mediate CIL (Figure 5-figure supplement 1d and Figure 5-Video 1**)**. To test this, we performed immunostaining of control and N-cadherin knockdown cells. Consistent with mRNA and protein analysis, total levels of Slit2 and Slit3 staining were unchanged following N-cadherin knockdown (Figure 5-figure supplement 1e-g). Confocal images of control-treated SCs showed that Slit2 and Slit3 were localised at the membrane in both free moving cells and cells in contact (Figure 5-figure supplement h) and could be detected at lamellipodia (Figure 5a-d). Moreover, both ligands could be detected in numerous vesicles throughout the cytoplasm. In contrast, in N-cadherin knockdown cells, Slit2 and Slit3 were no longer observable at the cell-surface but rather were sequestered in the perinuclear region (Figure 5a, c and quantified in Figure 5b,d). Importantly, Slit2 and Slit3 localisation could be restored by expression of the extracellular domain of N-cadherin (Figure 5e, g and quantified in Figure 5f,h). In contrast, Slit2 and Slit3 were still observed at the cell surface in Glypican-4 knockdown cells, suggesting Glypican-4 does not have a role in trafficking Slit2/3 to the cell-surface but more likely has a role in stabilising the cell-surface presentation, as indicated by previous studies (Ronca et al., 2001) (Figure 5-figure supplement). Together these results show that a pool of N-cadherin, via its extracellular domain, is required to facilitate Slit2 and Slit3 localisation at the cell-surface, where, together with Glypican-4, they mediate CIL.

The Slit repulsive signal is required for the efficient collective migration of Schwann cells

CIL can provide an outward force in collectively migrating cells (Roycroft et al., 2018; Scarpa et al., 2015; Theveneau et al., 2010). To test if the Slit CIL signal is important for the collective migration of SCs, we performed a collective migration assay with Slit2/3 KD SCs and found this was sufficient to decrease the collective migration of these cells (Figure 6a, Figure 6-figure

supplement 1a and Figure 6-Video 1). The ability to inhibit the CIL signal whilst maintaining cell: cell contacts has therapeutic potential in that rather than producing overlapping cells (N-cadherin inhibition) it should result in the formation of more tightly clustered, less migratory cells. Recombinant Slit2 (rSlit2), has been reported to induce a repulsive signal associated with a collapse of protrusions (Wang et al., 2013), and thus could potentially act in a dominant-negative manner by providing a uniform signal around cells. To test this, we initially analysed the effect of rSlit2 on CIL in low density cultures and found that rSlit2 inhibited Slit-mediated repulsion signalling, as rSlit2-treated SCs no longer repulsed each other and instead formed clusters (Figure 6b, quantified in 6c and Figure 6-Video 2), similar to that observed when Slit signalling was inhibited using siRNA (Figure 4e). Next, we performed a collective migration chamber assay in cells treated with rSlit2 and found that similar to the Slit2/Slit3 knockdowns, cells treated with rSlit2 migrated less efficiently than controls, with a slower closure of the gap (Figure 6d, Figure 6-figure supplement 1b and Figure 6-Video 3). By tracking the individual cells, we observed this behaviour was distinct from N-cadherin knockdown cells in that the cells migrated a shorter distance (Fig 6e-f) and appeared to adhere to each other, which prevented them from migrating forward, consistent with the loss of repulsion signal observed when Slit2/Slit3 signalling is inhibited at low density (Figure 6b-c and 4d-e).

SCs migrate collectively as cords during nerve regeneration in response to a Sox2 signal that results in the formation of more stable N-cadherin junctions, which is dominant over the CIL signal (Parrinello et al., 2010). Loss of the CIL signal should therefore maintain these junctions while blocking the outward force required for collective migration. Consistent with this, we found that the addition of rSlit2 to Sox2-induced SC clusters resulted in clusters with a distinct morphology (Figure 6g), in that the clusters were rounder (Figure 6-figure supplement 1 d-e), and that the cells within the cluster lacked polarisation away from the cluster, as measured by both cell roundness (Figure 6h) and nuclear alignment (Fig Figure6i and Figure 6-figure supplement 1d), suggesting a lack of repulsion between the cells (Astin et al., 2010). Moreover, loss of Slit2/Slit3 in Sox2-induced SC clusters resulted in a similarly profound change in cluster morphology with

the formation of large, round, clusters that lacked polarity in contrast to the polarised clusters of cells that form in response to Sox2 (Figure 6j, quantified in 6k and Figure 6-figure supplement 1f-g). Together these findings indicate that the outward force provided by Slit2/Robo signalling is required for SC collective migration and that inhibiting this signal results in the formation of non-polarised clusters of cells with limited migratory ability (Figure 6l).

To confirm these findings within the context of the nerve environment, we developed a novel ex-vivo explant system which allowed live visualisation of SC migration within the regenerating bridge region, following injury. This involved the use of transgenic mice in which eGFP is expressed in SCs (PLP-eGFP) allowing the visualisation of SCs within the complex environment of the nerve bridge (Mallon et al., 2002). Nerves were removed at Day 5 following a transection injury, at which point SC cords are migrating into the new tissue formed at the injury site (the nerve bridge). The nerves were removed in defined conditions that allowed the survival of the cells within the nerve bridge ex-vivo for up to 24 hours (Figure 7a). Nerves were embedded in agarose and sections of the bridge cut on a vibratome and imaged prior to treatment (0h), before slices were incubated overnight with PBS or rSlit2. The following day (24h), slices were fixed and imaged to compare the effect of inhibition of Slit2 on migration. We observed that the structure of the injured nerve was maintained ex vivo, with the bridge comprising of densely packed nuclei, with regrowing axons migrating on the surface of SC cords along the newly-formed vasculature (Figure 7b, Figure7-figure supplement 1 a-b), indicating that this is a powerful model in which we can visualise nerve regeneration ex vivo (Cattin, 2015, Parrinello, 2010).

At day 5 post-injury, at 0h, SCs cords could be visualised beginning to migrate from the stumps into the newly formed nerve bridge (Figure 7-figure supplement 1c). Moreover, at 24 hours, the polarised cords of SCs had further migrated across the bridge in the PBS treated explants, (Fig 7c, Figure 7-figure supplement 1c. Figure 7-Video 1). In contrast, treatment with rSlit2 resulted in an impairment of the collective migration of SCs, as evidenced by a decrease in the area of SC migration at 24 hours (Figure 7c-d). Moreover, within rSlit2 treated nerves, the SCs exhibited a distinct morphology in that there were significantly fewer SCs in polarised cords (Figuree-f) with

the SCs instead, found in clusters, comparable in phenotype to those seen in vitro (Figure 7g). Further analysis of the SCs within the bridge, using Imaris to define the individual shape of the cells, showed that those treated with rSlit2 displayed a more rounded phenotype when compared to controls, consistent with the loss of CIL between the SCs resulting in a loss of polarisation (Figure 7h-i). As an additional measurement of persistence of directionality, we measured, the alignment of the following cell to the leader cells and found increased alignment in the control cells, consistent with polarised collective migration (Figure 7j and Figure 7-figure supplement 1d). Moreover we also found the control cords were more aligned as they migrated across the wound site, whereas the rSlit2 treated explants appeared to lose this directionality, resulting in SCs migrating in more random directions into the bridge (Figure 7k). Together, these findings confirm the importance of the Slit2 mediated CIL signal for the effective migration of SC cords, which are essential for nerve regeneration. Moreover, these studies explain the apparently opposing dual roles for N-cadherin in the collective migration of SC during nerve regeneration, in that N-cadherin acts at SC cell:cell junctions to mediate the formation of migratory SC cords, whilst acting as a mediator of the repulsive Slit/Robo CIL signal to provide the force required to drive the outward migration of the SC cords that ensures successful nerve repair (Figure 7l).

Discussion

SCs migrate collectively as cellular cords following the severing of a peripheral nerve, guiding regrowing axons back to their targets, and thereby promoting peripheral nerve regeneration (Cattin et al., 2015; Cattin & Lloyd, 2016; Parrinello et al., 2010; Stierli et al., 2018). Collective migration is a complex and continuously adapting process that requires the incorporation of multiple and opposing intercellular signals between individual cells within the group, as well as signals from the local environment such as chemotactic factors, which guide and induce migration, while repulsion signals from surrounding cells prevent the migrating cells invading tissues (Haeger et al., 2015; Mayor & Etienne-Manneville, 2016). During migration, intercellular-repulsive signals direct the migration of the cluster forward, whilst adhesive interactions are needed to maintain a cohesive

group. How these seemingly opposing forces are co-ordinated to achieve collective migration remains mostly unclear (Haeger et al., 2015; Mayor & Etienne-Manneville, 2016).

We previously showed that, similarly to other cell-types such as astrocytes and neural crest cells (Etienne-Manneville, 2014; Peglion et al., 2014; Theveneau et al., 2010), the adherens junction molecule N-cadherin is required for SC collective migration by mediating the clustering of the SCs (Parrinello et al., 2010). In this study, we show that N-cadherin is also required for the repulsion signal, which provides an outward force for collective SC migration. N-cadherin has previously been shown to mediate the repulsion signal important for the collective migration of neural crest cells (Becker et al., 2013; Scarpa et al., 2015; Theveneau et al., 2010). However, despite neural crest cells and SCs belonging to the same lineage, we find that N-cadherin acts by a different mechanism to regulate CIL in SCs; CIL between neural crest cells was reported to require the trans-homodimerisation of N-cadherin that acted to inhibit local protrusion formation at cell-cell contacts via the adherens complex (Becker et al., 2013; Scarpa et al., 2015; Theveneau et al., 2010). In contrast, in SCs, while cell-cell adhesion is mediated by N-cadherin homodimers linked to the actin cytoskeleton via the adherens junction complex, N-cadherin mediates CIL by a distinct mechanism. This does not require trans-homodimerisation, is independent of the adherens junction complex and only requires the extracellular-domain. Instead, N-cadherin is required for the Slit2/Slit3 repulsion signal to be present at the cell surface (Figure 7h). The reasons for these differences remain unclear but could reflect that whereas SCs migrate in cordlike structures, neural crest cells migrate in much looser clusters, which appears to involve a co-attraction mechanism to maintain a migratory cluster (Carmona-Fontaine et al., 2011; Shellard & Mayor, 2020).

Slits are secreted axonal guidance molecules that are crucial for the development of the brain (Blockus & Chedotal, 2014; Brose et al., 1999; Gonda et al., 2020; Jia et al., 2005; Kidd et al., 1999; Nguyen-Ba-Charvet et al., 2004; Ypsilanti et al., 2010). However, while secreted, accumulating evidence suggests that the secreted forms can remain associated with the plasma membrane which would allow the local cell-cell signalling required for CIL (Blockus & Chedotal, 2016) indeed, it has been reported that CIL between fibroblasts involves Slit2/Robo4 signalling

(Fritz et al., 2015). Here, we show that Slit2/Slit3 signalling is responsible for the homotypic CIL signal between SCs and that this signal is required for the efficient directional collective SC migration that is required for nerve repair. This is consistent with reports that Slit2, Slit3 and Robo1 are expressed by myelinating and non-myelinating SCs (Carr et al., 2017; Wang et al., 2013) and that a Slit2 signal can repulse a SC in culture (Wang et al., 2013). The ability of a secreted Slit signal to act as a repellent over both longer and short distances, likely requires cell-specific mechanisms that regulate whether the Slit molecules remain tethered to the cell surface (Simpson, Bland, et al., 2000; Simpson, Kidd, et al., 2000). Our work shows that Slit-dependent CIL between SCs requires both the extracellular domain of N-cadherin and Glypican-4, and it therefore appears likely that this complex is important for the localisation and retention of Slit2/Slit3 at the cell-surface. This is consistent with previous reports in which Glypican and other heparan sulfate proteoglycans appear to be important for local Slit signalling (Liang et al., 1999; Piper et al., 2006; Ronca et al., 2001). We show that Slit2/3 protein localisation is dependent on N-cadherin, indicating a role for N-cadherin in the presentation of Slit2/3 at the cell membrane. Interestingly, we did not detect an obvious difference in Slit2 membrane staining between SCs in contact and free moving SCs, which might suggest Slit2 is constantly presented at the cell surface, although this remains to be fully established (Figure 5-figure supplement 1g). The absence of Slit2/3 in vesicles following N-cadherin knockdown would suggest N-cadherin is required for Slit2/3 delivery to the membrane, rather than effects on recycling, but further work is required to establish the precise mechanism by which N-cadherin mediates the localisation of Slit2/3 at the cell surface. Interestingly, Robo1/2 localisation does not appear to be dependent on N-cadherin expression, as our mixing experiments (Figure 2a-b) show that N-cadherin knockdown cells are still repulsed by a control cell, implying that Robo1/2 are still capable of enacting a repulsion signal in the absence of N-cadherin.

Further complexities of the role of CIL in cell behaviour are indicated by the distinct mechanisms used to regulate heterotypic and homotypic CIL and how these signals can change the migratory behaviour of cells. SCs show complex migratory behaviours influenced by the microenvironment;

SCs alone exhibit CIL, which we now show is a N-cadherin/glypican4/ Slit2/Slit3 /Robo1/2 dependent process that repulse SCs from each other, which is perhaps important for the distribution of SCs along axons. Following an injury however, SCs come into contact with fibroblasts at the injury site and the fibroblasts repulse SCs by an ephrinB/EphB2–dependent signal (Parrinello et al., 2010). Importantly, this signal also changes the behaviour of N-cadherin resulting in the formation of more stable N-cadherin junctions via Sox2. Critical to this interaction is the dual role of N-cadherin in SC migration, with Sox2 mediated stabilisation of N-cadherin at the cell-cell contacts found to act dominantly over the CIL signal, resulting in the formation of cellular cords. However, within the cords, the Slit2/Slit3-dependent repulsion signal remains active, providing an outward force to drive the collective migration of these cells. While both N-cadherin and Slit2/Slit3 are important for the collective migration of cells, inhibition of these proteins has very distinct effects on the migration of SCs. So, whereas loss of N-cadherin results in the production of invasive, highly-migratory cells that lack collective behaviour, inhibition of Slit2/Slit3 results in the formation of tighter clusters of cells associated with enhanced N-cadherin junctions in which migration is inhibited (Figure 6k)**.** This might suggest targeting of CIL signals would be a promising approach for inhibiting collective migration. Consistent with this, we showed that exogenous recombinant Slit2 (rSlit2) acts to inhibit SC CIL and inhibits the collective migration of these cells. Moreover, this effect could be reproduced in a powerful new ex vivo explant model, where we observed a similar phenotype with the failure to form cell cords associated with decreased migration, showing the Slit CIL signal is required for efficient SC migration within the context of a regenerating nerve environment (Figure 7b-c). This failure to form polarised cords is consistent with reports that collective cell migration relies on the polarisation of the cell group in the direction of migration and the transmission of forces between the cell-cell contacts (Capuana et al., 2020; Etienne-Manneville & Arkowitz, 2020). The crucial role of collective migration has been well established in tumour cell migration and metastasis, with a role proposed for CIL in this process (Abercrombie, 1979; Astin et al., 2010; Batson et al., 2014; Hwang et al., 2023; Jahedi et al., 2023; Paddock & Dunn, 1986). Characterisation of CIL

473 signals in distinct tumour types may therefore be a promising approach to identify new targets for
474 inhibiting the invasion and spread of tumours.
475
476
477

Materials and Methods

Animals

All animal work was performed in accordance with the UK Home Office legislation. Mice were group housed in temperature-controlled conditions on a 12 hour light-dark cycle with free access to food and water. To visualise SCs for ex vivo imaging, female and male (6-12 weeks old) plp-eGFP (Mallon et al., 2002) mice were used, in which SCs express eGFP.

Sciatic Nerve Injury

Sciatic nerve injury was performed under aseptic conditions with Isoflurane anaesthesia. Briefly, an incision was made, the right sciatic nerve exposed at the sciatic notch and a full transection performed. The wound was then closed with surgical clips and the animal allowed to recover. For ex vivo imaging experiments, sciatic nerves were harvested at Day 5 post injury.

Ex vivo imaging

Sciatic nerves were harvested on day 5 post sciatic nerve injury and collected on ice in EBSS dissection buffer (EBSS no phenol red (Gibco), 2nM Ascorbic Acid, Hepes, 18mM Glucose, 1.3mM $MgSO_4$, 2nM $CaCl_2$). Next, nerves were placed in 3% low melting point agarose (Invitrogen) and the gel allowed to polymerise. Once the gel was set, 150 um sections of nerve were cut on a Vibratome (Leica) in cold EBSS sectioning buffer (EBSS phenol red (Gibco), 2mM Ascorbic Acid, 13.1mM Glucose, Penicillin/Streptomycin (Gibco)), sections were collected and stored on ice. Once sectioning was complete, nerves were mounted on 35mm glass bottom dishes (MatTek) using a mix of 1.5% low melting point agarose and SC ex vivo media (Ham's F12 media (Gibco), 20ng/ml ß- neuregulin (R&D), 100 uM cAMP (Sigma), 5% Horse Serum, Penicillin/Streptomycin, 100ug/ml Transferrin, Insulin (Sigma)). Tile scan images of the nerve bridge were acquired prior to treatment at 0h (Leica TCS SP8 STED) at 37ºC, 10% CO_2. Sections were randomly divided into experimental groups and PBS or rSlit2 (40ug/ml) was added blind to the ex vivo media and sections placed in the incubator at 37ºC, 10% CO_2 for 24 hours. Explants were then fixed with 4% PFA and nuclei labelled with Hoechst before tile scan images were

acquired to assess migration at 24 hours. For live imaging, sections were imaged on the Leica TCS SP8 STED at 37ºC, 10% CO_2 every 15 minutes for up to 24 hours.

Ex vivo image analysis

To quantify SC migration in ex vivo explants, maximum projection tile scan images from the bridge at Day 5 were acquired by confocal microscopy (Leica TCS SP8 STED). To quantify the area of SC migration, a horizontal line was drawn to demarcate the boundary between the stump and the bridge and the area of SCs labelled with plp-eGFP was drawn using FIJI at 0, and 24 hours on. Data were expressed as area fold change in migration from 0h for each individual animal. To calculate the percentage of SC in cords or clusters, sections were stained with Hoechst for 30' after fixation. Total SC nuclei were counted based on overlap with plp-eGFP and SC morphology, and the number of SC in cords or clusters recorded. A cord was defined as two or more aligned SC migrating into the bridge. A cluster was defined two or more non polarised SC. In order to calculate cell roundness, images of the bridge following 24h of treatment were opened on Imaris (V9.1.2). Surfaces were created for SCs (plp-eGFP) and nuclei (Hoechst), and segmented so individual SCs could be identified in the nerve bridge, and the values for cell sphericity recorded. The same surface creation parameters were used for all images within an experiment, with minor adjustments in intensity threshold made to compensate for intensity differences between experiments. To calculate ex vivo SC persistence more directly, the same surface images were opened in Fiji and the angle of SC cords was measured relative to the stump and the angle of deviation from directional migration calculated. The same images were used to calculate the persistence of migration within each cord, with the angle of the nuclei measured in Fiji and calculated relative to the angle of the nuclei of the leading cell as an indicator of cell persistence (Supplementary Figure 6d).

Cell culture

Primary rat Schwann cells (SCs) were extracted from sciatic nerves of Sprague Dawley rats at postnatal Day 7 as previously described(Mathon et al., 2001). SCs were cultured on poly-L-lysine

(PLL) coated dishes in Dulbecco's Modified Eagle's Medium (DMEM, Lonza) supplemented with 3% Fetal Bovine Serum (FBS, BioSera), 1μM Forskolin (Abcam), 200mM L-Glutamine (Gibco), GGF, 100μg/ml Kanamycin (Gibco) and 800μg/ml Gentamicin (Gibco) and maintained in 10% CO_2 at 37ºC. HEK293T cells were cultured in DMEM (Lonza) supplemented with 10% FBS and 200mM L-Glutamine (Gibco).

Sox2 overexpressing SCs were produced using the Retro X ProteoTuner Shield system (Clontech). The Retro X ProteoTuner retroviral vector encodes a 12kDa FKBP destabilization domain (DD) that causes rapid degradation of the protein to which it is fused. The DD domain was fused to mouse Sox2 cDNA at the N-terminus. Accumulation of the DD tagged protein was induced by addition of Shield1 (Takara Bio) stabilising ligand to the media, which prevents the proteasomal degradation of the protein. For analysis of Sox2 clusters, Shield1 (200nM) was added to Sox2 overexpressing SC or ProteoTuner SC controls and cells fixed 24h following treatment.

Cells for cell clustering or collective migration assays, were pre-treated with 2μg/ml recombinant mouse Slit2 protein (rSlit2) (R&D system, 5444-SL-050) or PBS for 18 hours before time-lapse microscopy and/or fixation.

Constructs

N-cadherin full length, the extracellular and intracellular domain of N-cadherin tagged with Tomato on the C-terminus, were a kind gift from Prof. S. Yamada(Shih & Yamada, 2012). The myc-tagged Slit2 construct was a gift of Dr. V. Castellani (Delloye-Bourgeois et al., 2015).

Antibodies

Primary antibodies were used that recognise N-cadherin (BD transduction); α-catenin (Sigma C2081); β-catenin (BD transductions 610920); p120-catenin (BD Transduction 61034); ERK1/2 (Sigma M5670), mCherry (Abcam ab183628; Western blotting); mCherry (Life technologies M11217; Immunoprecipitation), AKT 1/2/3 (Santa Cruz), Slit2 (Abcam ab134166; Western blotting), Slit2 (Thermo Fisher Scientific PA531133; Immunofluorescence), Slit3 (Sigma SAB2104337; Immunofluorescence) Slit3 (R&D Systems AF3629; Western blotting), Myc (Merck

559 Millipore 05-724). Alexa-Fluor secondary antibodies were obtained from Invitrogen. Horseradish
560 peroxidase (HRP)-linked antibodies were obtained from GE-healthcare.

561 ***Short interference RNA***

562 All short interference RNA (siRNA) were purchased from Qiagen, with All star control siRNA
563 (Qiagen) used a control. In brief, 10^5 cells SCs were seeded on 6 well plates. The following day
564 siRNA or control siRNA were mixed in plain DMEM with HiPerFect (Qiagen) and incubated for
565 10 min at room temperature (RT) to allow complexes to form. Complexes were added to SCs for
566 16-18 hours, washed once with SC medium and harvested or seeded for further experiments as
567 appropriate.

568 ***Mutagenesis***

569 To disrupt the annealing of N-cadherin siRNA to the tomato-tagged N-cadherin full-length, or the
570 extracellular domain of N-cadherin constructs, the NEB Q5 Site-Directed Mutagenesis Kit (NEB)
571 was used to introduce silent mutations in the N-cadherin siRNA1 targeting sequence, which is
572 located in the extracellular domain of N-cadherin, by mutating all four codons of the target
573 sequence.

574 ***Protein Analysis***

575 For protein extraction, cells were washed on ice with PBS, followed by snap-freezing at -80ºC to
576 break membranes and harvested in RIPA buffer (1% Triton X-100, 0.5% sodium deoxycholate,
577 50mM Tris pH7.5, 100mM NaCl, 1mM EGTA pH8, 20mM NaF, 100µg/ml PMSF, 15µg/ml
578 aprotonin, 1mM Na_3VO_4, 1/100 protease inhibitor cocktail). Cells were then lysed on ice for 30
579 min, vortexed every 10 min and homogenised using a 26-gauge needle (Beckton Dickinson). Cell
580 debris was pelleted by spinning at 750-g for 5 min at 4ºC, and the supernatant was collected and
581 quantified using the BCA assay (Pierce, Thermo Scientific).

582 ***Western Blotting***

583 Western blotting was performed using Hoefer Scientific Instrument apparatus and Bio-Rad
584 western blot electrophoresis system. 20 to 30µg of protein was resolved using a Sodium Dodecyl
585 Sulfate-polyacrylamide gel electrophoresis (SDS-PAGE). Protein was transferred onto

nitrocellulose membrane (Millipore-Immobilon) and blocked for one hour at RT using 5% milk-TBST. The membrane was incubated with primary antibodies overnight at 4ºC. The following day, the membrane was washed three times with TBST, followed by incubation with the appropriate HRP conjugated secondary antibody. Subsequently, membranes were washed three times with TBS-T before detection of proteins of interest with Pierce-ECL Western blot substrate (Thermo Scientific) or Luminata Crescendo Western HRP substrate (EMD-Millipore) on the Imagequant LAS 4000.

Transfection of HEK293T cells

DNA was transfected using Attractene according to the manufacturer's instructions (Qiagen). Briefly, HEK293T cells were seeded onto 60mm plates 24 hours prior to transfection. 270ng Myc tagged Slit2 and 270ng of Tomato-tagged constructs of interest and 1.25µg carrier vector DNA was incubated with Attractene in DMEM for 15 min at RT to allow complexes to form. Complexes were incubated for 2 hours at 37ºC. Cells were harvested after 48 hours for coimmunoprecipitation (Co-IP).

Co-immunoprecipitation

HEK cells were seeded at $1.2x10^6$ onto 60mm dishes and transfected as described above. Cells were scraped in NP40 buffer (50mM Tris pH 7.5, 150mM NaCl, 1% NP40 supplemented with 1/100 protease cocktail inhibitor (Sigma), 1/100 phosphatase inhibitor cocktail 2 and 3 (Sigma)), lysed on ice for 30 min. Debris was pelleted, by centrifuging at 750-g for 5 min at 4ºC and the supernatant was collected into a fresh tube. Protein concentration was then quantified using BCA assay. All subsequent steps were performed at 4ºC. Approximately 1mg protein was pre-cleared using 10µl of 50% protein G Beads (GE healthcare) by rotating for 15 min. Beads were collected and discarded by centrifuging at 750-g for 1 min. Pre-cleared supernatant was incubated with primary antibodies to Tomato (7ug of anti-mcherry (life technologies)) or Rat IgG as a control (life technologies) for 2 hours, rotating. The antibody-protein complexes were isolated by rotating the mixture with 50µl of 50% Protein G beads for 1 hour. Beads were washed 4 times with 500µl NP40 buffer and were collected by centrifugation at 750-g for 1 min and transferred to a clean

tube. Finally, the beads were resuspended in 30µl of Laemlli buffer and boiled for 10 minutes at 95ºC.

To identify the homotypic CIL signal, we performed a series of proteomic screens, using N-cadherin or the extracellular domain of N-cadherin as bait, followed by co-immunoprecipitation and mass spectrometry analysis. To do this, cells which displayed repulsion and overlapping behaviours were used to identify a signal that was only present in the repulsing cells. The Co-IP was performed on one sample per condition using 1mg protein as input, and the proteins eluted from the beads using Laemmli buffer. The proteins were then separated on a gel, extracted, digested with trypsin and analysed using the LTQ Orbitrap Velos Pro Mass-spec systems (Performed by Proteomics Facility, University of Dundee). The obtained data was analysed using the Mascot search engine using the Uniprot DB with rat as the taxonomic filter (performed by the Proteomics Facility, University of Dundee).

RNA extraction and qPCR

RNA extraction was performed using Tri-Reagent according to the manufacture's protocol. RNA concentration was determined using Nanodrop and 500-1000ng of RNA was used to synthesise complementary DNA using Superscript II kit (Invitrogen). For RT-qPCR the MESA Blue qPCR MasterMix Plus kit was used (Eurogentec).

Migration Assays

Contact inhibition of Locomotion assays

For repulsion assays $8x10^3$ or $4x10^3$ control or siRNA-treated SCs were seeded onto PLL and laminin coated 6 well plates or 12 well plates respectively. Cells were allowed to adhere for a minimum of 6 hours and then time-lapse microscopy was performed. Live imaging was performed using a Zeiss Axiovert 200M microscope or the Nikon GFP3 at 37ºC with 5- 10% CO_2. Images were taken every 10 minutes for up to 72 hours.

To analyse interactions between control and N-cadherin knockdown cells, cells were treated with 10μM Cell Tracker Red CMTPX Dye or Green CMFDA dye (Invitrogen) for 30 min at 37°C and washed once with SC medium. Following 1 hour incubation with Cell Tracker, 4 $x10^3$ control cells were mixed with 4 $x10^3$ N-cadherin knockdown cells and incubated for 16 hours before time-lapse microscopy.

Volocity or Fiji software was used to quantify repulsion. Single cells that were not dividing were tracked until contact with another cell and the initial response upon contact recorded. Three types of events were defined: Retraction, cells retract protrusions and change direction of migration; No-retraction, cells interact for longer than five hours and don't change the direction of migration; overlapping, cell migrate on top of another cell with their protrusion and/or cell bodies.

For mixing experiments, the response of control-treated cells, was quantified upon contact with N-cadherin knockdown cells and vice versa. Similarly, for rescue experiments only the response of N-cadherin knockdown cells was quantified upon contact with a cell expressing either GFP, full length N-cadherin, the extracellular domain of N-cadherin or the intracellular domain of N-cadherin. To quantify the displacement of a cell after contact, vector analysis was used to analyse interactions between migrating cells. Videos were opened in Fiji and the displacement of a migrating cell 15 minutes prior to (Vector A) and following a collision (Vector B) calculated (Paddock & Dunn, 1986). The difference in displacement between the vectors (Vector B-A) was calculated to analyse the difference between how far the cell has progressed and how far it would have migrated had it not encountered another cell. Free moving cells which did not collide with other cells were also analysed over the same duration. Cells exhibiting CIL have a negative value indicating that the cell has changed direction following collision.

Rescue experiments

Rescue experiments were performed in a two-step protocol, first siRNA transfection was performed using 1nM of N-cadherin siRNA1 as described above and incubated overnight. The following morning, the complexes were removed, and 4 hours later full length N-cadherin, the extracellular domain of N-cadherin or the intracellular domain of N-cadherin were transfected

using Attractene (Qiagen). Complexes were incubated with control or N-cadherin knockdown cells for 2 hours at 37ºC. The following day, cells were seeded for repulsion assays and immunofluorescence.

Time-lapse microscopy was performed approximately 6 hours after seeding for 24 hours.

Collective migration assays

For collective migration assays, two approaches were taken. Either (i) $1x10^5$ cells were seeded onto laminin-coated plates and the following day, siRNA transfection was performed as described above. A scratch was then induced with a sterile tip, 48 hours after knockdown. The cells were gently washed twice with medium to remove any debris followed by time-lapse microscopy of the leading edges for 24 hours. Or (ii) $1.5x10^4$ Control or knockdown cells were seeded into the separate compartments of dual-chamber inserts (Ibidi), 24 hours after siRNA transfection. The following morning, each compartment was treated with CellTracker-Green or Cell Tracker Red CMTPX Dye, for 30 min. Subsequently, the chamber was removed, and cell migration imaged using time-lapse microscopy for 24 hours on the Nikon GFP3 at 37ºC, 10% CO_2. In order to quantify collective migration, the area of cells was drawn using FIJI at 0, 6 or 24 hours on stills from time-lapse microscopy. The area migrated was calculated using the formula:

$$\text{Area migrated} = \text{Area } 0 + \text{Xh} - \text{Area } 0\text{h}$$

Data were expressed as area fold migration change relative to PBS or control siRNA.

Cell tracking

Cells were tracked by their nucleus using Volocity software or the manual cell tracking plugin in FIJI for 8-12 hours (dividing cells were excluded). Velocity and directionality were then measured from the tracks using macro plugin in Excel as described in (Gorelik & Gautreau, 2014).

Cell clustering assays

Cell clustering assay was performed as described in (Parrinello et al., 2010). Briefly, 3.5 x 10^3 cells treated with Glypican-4, Robo1/2 or Slit2/3 siRNA were seeded onto coverslips 48 hours after knockdown. Clusters were fixed 24 hours after seeding, and immunofluorescence performed as described below. For rSlit2 treated cells, 5 x 10^3 cells were seeded onto a 12 well plate and clusters quantified after 36 hours of treatment. The following clusters were defined, single cells, 2, 3, or >4 cells.

Immunofluorescence

Cells grown on glass coverslips were fixed in 4% paraformaldehyde (PFA) supplemented with 1mM $CaCl_2$ and 0.5mM $MgCl_2$ to prevent disruption of calcium-dependent complexes such as N-cadherin, for 10 min at room temperature (RT). Cells were then permeabilised with 0.3% Triton PBS for 10 min and blocked with 3% Bovine serum albumin-PBS (BSA) for 1 hour at RT and incubated with primary antibodies overnight at 4ºC. The following day, coverslips were washed with PBS, incubated with the appropriate secondary antibodies for one hour at RT and washed with PBS before mounting onto microscope slides using fluoromount-g (Southern Biotech).
For labelling of Slit2 and Slit3, cells were fixed in 2% PFA supplemented with 1mM $CaCl_2$ and 0.5mM $MgCl_2$ and blocked in 3% BSA. All remaining steps were performed as described above. All images were acquired using an inverted Leica TCS SPE confocal microscope, with image processing and analysis performed using FIJI software.

Quantification of immunofluorescence

To quantify Slit3 and Slit2 immunolabelling, the outline of the cells was drawn using the free-hand drawing tool in Fiji and the fluorescence intensity was measured using Fiji. The nucleus and perinuclear area were excluded from the quantification in order to calculate the intensity in the protrusions. In order to quantify the roundness of individual SCs in clusters or the roundness of the entire cluster, the following equation was used:

$$\text{Shape} = 4\Pi x \text{Area}/\text{Perimeter}^2$$ (Rotty et al., 2017)

where the area and perimeter of each cell was measured by tracing their outline using FIJI from confocal images. Groups of SCs were considered to be in clusters if they consisted of >4 cells. To further quantify polarity of the clusters, images were opened in Fiji and the angle of the cluster in the direction of movement measured. The nuclei of each cell in the cluster was also measured, and the angle relative to the cluster axis calculated. Data was then imported into MATLAB to generate polar histogram plots.

Statistics

Statistics were performed using GraphPad (Prism) software. Data is presented as mean ±SEM and is representative of at least n=3 independent experiments. Data were analysed using a one-way or two-way analysis of variance (ANOVA), followed by multiple comparisons tests, two-tailed unpaired Student's t-test with Welch's correction or Mann-Whitney test as appropriate and are detailed in the figure legends. In all cases p *< 0.05, **<0.01, *** <0.001.

Acknowledgements

This work was supported by a programme grant from Cancer Research UK (C378/A4308), a MRC PhD studentship to J.J.A.H and core support by MRC funding to the MRC LMCB University Unit at UCL, award code MC_U12266B. We would like to thank UCL Biological Services for helping with the maintenance of our animals, Giulia Casal for useful advice on image analysis and Imaris, Lucie Van Emmenis and Stella Kouloulia for assistance with surgeries, Liza Malong for her input regarding the ex vivo protocol, and the rest of the Lloyd lab for useful discussions.

Competing interests

The authors declare no competing financial interests. Correspondence and requests for materials should be addressed to A.C.L. (alison.lloyd@ucl.ac.uk).

Author contributions

A.C.L and J.J.A.H conceived the project and together with E.H-W wrote the manuscript and made the figures. J.J.A.H, E.H-W, A.C and A.C.L designed the experiments. J.J.A.H and E.H-W, performed the majority of experiments with help from P.W-D, A.C, M.C, E.T, A.P, V.Q and T.M.

References

Abercrombie, M. (1979). Contact inhibition and malignancy. *Nature*, *281*(5729), 259-262.

Abercrombie, M., & Heaysman, J. E. (1953). Observations on the social behaviour of cells in tissue culture. I. Speed of movement of chick heart fibroblasts in relation to their mutual contacts. *Exp Cell Res*, *5*(1), 111-131.

Abercrombie, M., & Heaysman, J. E. (1954). Observations on the social behaviour of cells in tissue culture. II. Monolayering of fibroblasts. *Exp Cell Res*, *6*(2), 293-306.

Astin, J. W., Batson, J., Kadir, S., Charlet, J., Persad, R. A., Gillatt, D., Oxley, J. D., & Nobes, C. D. (2010). Competition amongst Eph receptors regulates contact inhibition of locomotion and invasiveness in prostate cancer cells. *Nat Cell Biol*, *12*(12), 1194-1204. https://doi.org/10.1038/ncb2122

Batson, J., Maccarthy-Morrogh, L., Archer, A., Tanton, H., & Nobes, C. D. (2014). EphA receptors regulate prostate cancer cell dissemination through Vav2-RhoA mediated cell-cell repulsion. *Biol Open*, *3*(6), 453-462. https://doi.org/10.1242/bio.20146601

Becker, S. F., Mayor, R., & Kashef, J. (2013). Cadherin-11 mediates contact inhibition of locomotion during Xenopus neural crest cell migration. *PLoS One*, *8*(12), e85717. https://doi.org/10.1371/journal.pone.0085717

Blanchette, C. R., Perrat, P. N., Thackeray, A., & Benard, C. Y. (2015). Glypican Is a Modulator of Netrin-Mediated Axon Guidance. *PLoS Biol*, *13*(7), e1002183. https://doi.org/10.1371/journal.pbio.1002183

Blockus, H., & Chedotal, A. (2014). The multifaceted roles of Slits and Robos in cortical circuits: from proliferation to axon guidance and neurological diseases. *Curr Opin Neurobiol*, *27*, 82-88. https://doi.org/10.1016/j.conb.2014.03.003

Blockus, H., & Chedotal, A. (2016). Slit-Robo signaling [Review Research Support, Non-U.S. Gov't]. *Development*, *143*(17), 3037-3044. https://doi.org/10.1242/dev.132829

Brasch, J., Harrison, O. J., Honig, B., & Shapiro, L. (2012). Thinking outside the cell: how cadherins drive adhesion. *Trends Cell Biol*, *22*(6), 299-310. https://doi.org/10.1016/j.tcb.2012.03.004

Brose, K., Bland, K. S., Wang, K. H., Arnott, D., Henzel, W., Goodman, C. S., Tessier-Lavigne, M., & Kidd, T. (1999). Slit proteins bind Robo receptors and have an evolutionarily conserved role in repulsive axon guidance. *Cell*, *96*(6), 795-806.

Buckley, C. D., Tan, J., Anderson, K. L., Hanein, D., Volkmann, N., Weis, W. I., Nelson, W. J., & Dunn, A. R. (2014). Cell adhesion. The minimal cadherin-catenin complex binds to actin filaments under force. *Science*, *346*(6209), 1254211. https://doi.org/10.1126/science.1254211

Capuana, L., Boström, A., & Etienne-Manneville, S. (2020). Multicellular scale front-to-rear polarity in collective migration. *Curr Opin Cell Biol*, *62*, 114-122. https://doi.org/10.1016/j.ceb.2019.10.001

Carmona-Fontaine, C., Matthews, H. K., Kuriyama, S., Moreno, M., Dunn, G. A., Parsons, M., Stern, C. D., & Mayor, R. (2008). Contact inhibition of locomotion in vivo controls neural crest directional migration. *Nature*, *456*(7224), 957-961. https://doi.org/10.1038/nature07441

Carmona-Fontaine, C., Theveneau, E., Tzekou, A., Tada, M., Woods, M., Page, K. M., Parsons, M., Lambris, J. D., & Mayor, R. (2011). Complement fragment C3a controls mutual cell attraction during collective cell migration. *Dev Cell*, *21*(6), 1026-1037. https://doi.org/10.1016/j.devcel.2011.10.012

Carr, L., Parkinson, D. B., & Dun, X. P. (2017). Expression patterns of Slit and Robo family members in adult mouse spinal cord and peripheral nervous system. *PLoS One*, *12*(2), e0172736. https://doi.org/10.1371/journal.pone.0172736

Cattin, A. L., Burden, J. J., Van Emmenis, L., Mackenzie, F. E., Hoving, J. J., Garcia Calavia, N., Guo, Y., McLaughlin, M., Rosenberg, L. H., Quereda, V., Jamecna, D., Napoli, I., Parrinello, S., Enver, T., Ruhrberg, C., & Lloyd, A. C. (2015). Macrophage-Induced Blood Vessels Guide Schwann Cell-Mediated Regeneration of Peripheral Nerves. *Cell*, *162*(5), 1127-1139. https://doi.org/10.1016/j.cell.2015.07.021

Cattin, A. L., & Lloyd, A. C. (2016). The multicellular complexity of peripheral nerve regeneration. *Curr Opin Neurobiol*, *39*, 38-46. https://doi.org/10.1016/j.conb.2016.04.005

Chen, B., Carr, L., & Dun, X. P. (2020). Dynamic expression of Slit1-3 and Robo1-2 in the mouse peripheral nervous system after injury. *Neural Regen Res*, *15*(5), 948-958. https://doi.org/10.4103/1673-5374.268930

Davis, J. R., Huang, C. Y., Zanet, J., Harrison, S., Rosten, E., Cox, S., Soong, D. Y., Dunn, G. A., & Stramer, B. M. (2012). Emergence of embryonic pattern through contact inhibition of locomotion. *Development*, *139*(24), 4555-4560. https://doi.org/10.1242/dev.082248

Davis, J. R., Luchici, A., Mosis, F., Thackery, J., Salazar, J. A., Mao, Y., Dunn, G. A., Betz, T., Miodownik, M., & Stramer, B. M. (2015). Inter-cellular forces orchestrate contact inhibition of locomotion. *Cell*, *161*(2), 361-373. https://doi.org/10.1016/j.cell.2015.02.015

Davis, M. A., Ireton, R. C., & Reynolds, A. B. (2003). A core function for p120-catenin in cadherin turnover. *J Cell Biol*, *163*(3), 525-534. https://doi.org/10.1083/jcb.200307111

Delloye-Bourgeois, C., Jacquier, A., Charoy, C., Reynaud, F., Nawabi, H., Thoinet, K., Kindbeiter, K., Yoshida, Y., Zagar, Y., Kong, Y., Jones, Y. E., Falk, J., & Chedotal, A. (2015). PlexinA1 is a new Slit receptor and mediates axon guidance function of Slit C-terminal fragments. *18*(1), 36-45. https://doi.org/10.1038/nn.3893

Etienne-Manneville, S. (2014). Neighborly relations during collective migration. *Curr Opin Cell Biol*, *30*, 51-59. https://doi.org/10.1016/j.ceb.2014.06.004

Etienne-Manneville, S., & Arkowitz, R. (2020). Cell polarity inside-out. *Curr Opin Cell Biol*, *62*, iii-iv. https://doi.org/10.1016/j.ceb.2020.01.008

Friedl, P., & Gilmour, D. (2009). Collective cell migration in morphogenesis, regeneration and cancer. *Nat Rev Mol Cell Biol*, *10*(7), 445-457. https://doi.org/10.1038/nrm2720

Fritz, R. D., Menshykau, D., Martin, K., Reimann, A., Pontelli, V., & Pertz, O. (2015). SrGAP2-Dependent Integration of Membrane Geometry and Slit-Robo-Repulsive Cues Regulates Fibroblast Contact Inhibition of Locomotion. *Dev Cell*, *35*(1), 78-92. https://doi.org/10.1016/j.devcel.2015.09.002

Gonda, Y., Namba, T., & Hanashima, C. (2020). Beyond Axon Guidance: Roles of Slit-Robo Signaling in Neocortical Formation. *Front Cell Dev Biol*, *8*, 607415. https://doi.org/10.3389/fcell.2020.607415

Gorelik, R., & Gautreau, A. (2014). Quantitative and unbiased analysis of directional persistence in cell migration. *Nat Protoc*, *9*(8), 1931-1943. https://doi.org/10.1038/nprot.2014.131

Haeger, A., Wolf, K., Zegers, M. M., & Friedl, P. (2015). Collective cell migration: guidance principles and hierarchies [Research Support, Non-U.S. Gov't Review]. *Trends Cell Biol*, *25*(9), 556-566. https://doi.org/10.1016/j.tcb.2015.06.003

Harris, T. J., & Tepass, U. (2010). Adherens junctions: from molecules to morphogenesis. *Nat Rev Mol Cell Biol*, *11*(7), 502-514. https://doi.org/10.1038/nrm2927

Hwang, P. Y., Mathur, J., Cao, Y., Almeida, J., Ye, J., Morikis, V., Cornish, D., Clarke, M., Stewart, S. A., Pathak, A., & Longmore, G. D. (2023). A Cdh3-β-catenin-laminin signaling axis in a subset of breast tumor leader cells control leader cell polarization and directional collective migration. *Dev Cell*, *58*(1), 34-50.e39. https://doi.org/10.1016/j.devcel.2022.12.005

Jahedi, A., Kumar, G., Kannan, L., Agarwal, T., Huse, J., Bhat, K., & Kannan, K. (2023). Gibbs process distinguishes survival and reveals contact-inhibition genes in Glioblastoma multiforme. *PLoS One*, *18*(2), e0277176. https://doi.org/10.1371/journal.pone.0277176

Jessen, K. R., Mirsky, R., & Lloyd, A. C. (2015). Schwann Cells: Development and Role in Nerve Repair. *Cold Spring Harb Perspect Biol*, *7*(7), a020487. https://doi.org/10.1101/cshperspect.a020487

Jia, L., Cheng, L., & Raper, J. (2005). Slit/Robo signaling is necessary to confine early neural crest cells to the ventral migratory pathway in the trunk. *Dev Biol*, *282*(2), 411-421. https://doi.org/10.1016/j.ydbio.2005.03.021

Johnson, K. G., Ghose, A., Epstein, E., Lincecum, J., O'Connor, M. B., & Van Vactor, D. (2004). Axonal heparan sulfate proteoglycans regulate the distribution and efficiency of the repellent slit during midline axon guidance. *Curr Biol*, *14*(6), 499-504. https://doi.org/10.1016/j.cub.2004.02.005

Kaneko, N., Marin, O., Koike, M., Hirota, Y., Uchiyama, Y., Wu, J. Y., Lu, Q., Tessier-Lavigne, M., Alvarez-Buylla, A., Okano, H., Rubenstein, J. L., & Sawamoto, K. (2010). New neurons clear the path of astrocytic processes for their rapid migration in the adult brain. *Neuron*, *67*(2), 213-223. https://doi.org/10.1016/j.neuron.2010.06.018

Kidd, T., Bland, K. S., & Goodman, C. S. (1999). Slit is the midline repellent for the robo receptor in Drosophila. *Cell*, *96*(6), 785-794.

Klambt, C. (2009). Modes and regulation of glial migration in vertebrates and invertebrates [Comparative Study

Research Support, Non-U.S. Gov't

Review]. *Nat Rev Neurosci*, *10*(11), 769-779. https://doi.org/10.1038/nrn2720

Liang, Y., Annan, R. S., Carr, S. A., Popp, S., Mevissen, M., Margolis, R. K., & Margolis, R. U. (1999). Mammalian homologues of the Drosophila slit protein are ligands of the heparan sulfate proteoglycan glypican-1 in brain. *J Biol Chem*, *274*(25), 17885-17892.

Madsen, C. D., & Sahai, E. (2010). Cancer dissemination--lessons from leukocytes [Research Support, Non-U.S. Gov't

Review]. *Dev Cell*, *19*(1), 13-26. https://doi.org/10.1016/j.devcel.2010.06.013

Mallon, B. S., Shick, H. E., Kidd, G. J., & Macklin, W. B. (2002). Proteolipid promoter activity distinguishes two populations of NG2-positive cells throughout neonatal cortical development. *J Neurosci*, *22*(3), 876-885. https://doi.org/10.1523/JNEUROSCI.22-03-00876.2002

Mathon, N. F., Malcolm, D. S., Harrisingh, M. C., Cheng, L., & Lloyd, A. C. (2001). Lack of replicative senescence in normal rodent glia. *Science*, *291*(5505), 872-875. https://doi.org/10.1126/science.1056782

Mayor, R., & Etienne-Manneville, S. (2016). The front and rear of collective cell migration. *Nat Rev Mol Cell Biol*, *17*(2), 97-109. https://doi.org/10.1038/nrm.2015.14

Miyashita, Y., & Ozawa, M. (2007). Increased internalization of p120-uncoupled E-cadherin and a requirement for a dileucine motif in the cytoplasmic domain for endocytosis of the protein. *J Biol Chem*, *282*(15), 11540-11548. https://doi.org/10.1074/jbc.M608351200

Moreau, H. D., Piel, M., Voituriez, R., & Lennon-Dumenil, A. M. (2018). Integrating Physical and Molecular Insights on Immune Cell Migration [Review]. *Trends Immunol*, *39*(8), 632-643. https://doi.org/10.1016/j.it.2018.04.007

Nanes, B. A., Chiasson-MacKenzie, C., Lowery, A. M., Ishiyama, N., Faundez, V., Ikura, M., Vincent, P. A., & Kowalczyk, A. P. (2012). p120-catenin binding masks an endocytic signal conserved in classical cadherins. *J Cell Biol*, *199*(2), 365-380. https://doi.org/10.1083/jcb.201205029

Nguyen-Ba-Charvet, K. T., Picard-Riera, N., Tessier-Lavigne, M., Baron-Van Evercooren, A., Sotelo, C., & Chedotal, A. (2004). Multiple roles for slits in the control of cell migration in the rostral migratory stream. *J Neurosci*, *24*(6), 1497-1506. https://doi.org/10.1523/JNEUROSCI.4729-03.2004

Paddock, S. W., & Dunn, G. A. (1986). Analysing collisions between fibroblasts and fibrosarcoma cells: fibrosarcoma cells show an active invasionary response. *J Cell Sci*, *81*, 163-187.

Parrinello, S., Napoli, I., Ribeiro, S., Wingfield Digby, P., Fedorova, M., Parkinson, D. B., Doddrell, R. D., Nakayama, M., Adams, R. H., & Lloyd, A. C. (2010). EphB signaling directs peripheral nerve regeneration through Sox2-dependent Schwann cell sorting. *Cell*, *143*(1), 145-155. https://doi.org/10.1016/j.cell.2010.08.039

Peglion, F., & Etienne-Manneville, S. (2013). p120catenin alteration in cancer and its role in tumour invasion. *Philos Trans R Soc Lond B Biol Sci*, *368*(1629), 20130015. https://doi.org/10.1098/rstb.2013.0015

Peglion, F., Llense, F., & Etienne-Manneville, S. (2014). Adherens junction treadmilling during collective migration. *Nat Cell Biol*, *16*(7), 639-651. https://doi.org/10.1038/ncb2985

Piper, M., Anderson, R., Dwivedy, A., Weinl, C., van Horck, F., Leung, K. M., Cogill, E., & Holt, C. (2006). Signaling mechanisms underlying Slit2-induced collapse of Xenopus retinal growth cones. *Neuron*, *49*(2), 215-228. https://doi.org/10.1016/j.neuron.2005.12.008

Pokutta, S., & Weis, W. I. (2000). Structure of the dimerization and beta-catenin-binding region of alpha-catenin. *Mol Cell*, *5*(3), 533-543.

Poss, K. D. (2010). Advances in understanding tissue regenerative capacity and mechanisms in animals. *Nat Rev Genet*, *11*(10), 710-722. https://doi.org/10.1038/nrg2879

Reymond, N., d'Agua, B. B., & Ridley, A. J. (2013). Crossing the endothelial barrier during metastasis [Research Support, Non-U.S. Gov't
Review]. *Nat Rev Cancer*, *13*(12), 858-870. https://doi.org/10.1038/nrc3628

Rimm, D. L., Koslov, E. R., Kebriaei, P., Cianci, C. D., & Morrow, J. S. (1995). Alpha 1(E)-catenin is an actin-binding and -bundling protein mediating the attachment of F-actin to the membrane adhesion complex. *Proc Natl Acad Sci U S A*, *92*(19), 8813-8817.

Ronca, F., Andersen, J. S., Paech, V., & Margolis, R. U. (2001). Characterization of Slit protein interactions with glypican-1. *J Biol Chem*, *276*(31), 29141-29147.
https://doi.org/10.1074/jbc.M100240200

Rotty, J. D., Brighton, H. E., Craig, S. L., Asokan, S. B., Cheng, N., Ting, J. P., & Bear, J. E. (2017). Arp2/3 Complex Is Required for Macrophage Integrin Functions but Is Dispensable for FcR Phagocytosis and In Vivo Motility. *Dev Cell*, *42*(5), 498-513.e496.
https://doi.org/10.1016/j.devcel.2017.08.003

Roycroft, A., Szabo, A., Bahm, I., Daly, L., Charras, G., Parsons, M., & Mayor, R. (2018). Redistribution of Adhesive Forces through Src/FAK Drives Contact Inhibition of Locomotion in Neural Crest. *Dev Cell*, *45*(5), 565-579 e563. https://doi.org/10.1016/j.devcel.2018.05.003

Sarrazin, S., Lamanna, W. C., & Esko, J. D. (2011). Heparan sulfate proteoglycans. *Cold Spring Harb Perspect Biol*, *3*(7). https://doi.org/10.1101/cshperspect.a004952

Scarpa, E., & Mayor, R. (2016). Collective cell migration in development. *J Cell Biol*, *212*(2), 143-155. https://doi.org/10.1083/jcb.201508047

Scarpa, E., Szabo, A., Bibonne, A., Theveneau, E., Parsons, M., & Mayor, R. (2015). Cadherin Switch during EMT in Neural Crest Cells Leads to Contact Inhibition of Locomotion via Repolarization of Forces. *Dev Cell*, *34*(4), 421-434. https://doi.org/10.1016/j.devcel.2015.06.012

Shaw, T. J., & Martin, P. (2016). Wound repair: a showcase for cell plasticity and migration [Review]. *Curr Opin Cell Biol*, *42*, 29-37. https://doi.org/10.1016/j.ceb.2016.04.001

Shellard, A., & Mayor, R. (2020). Rules of collective migration: from the wildebeest to the neural crest. *Philos Trans R Soc Lond B Biol Sci*, *375*(1807), 20190387. https://doi.org/10.1098/rstb.2019.0387

Shih, W., & Yamada, S. (2012). N-cadherin-mediated cell-cell adhesion promotes cell migration in a three-dimensional matrix. *J Cell Sci*, *125*(Pt 15), 3661-3670. https://doi.org/10.1242/jcs.103861

Simpson, J. H., Bland, K. S., Fetter, R. D., & Goodman, C. S. (2000). Short-range and long-range guidance by Slit and its Robo receptors: a combinatorial code of Robo receptors controls lateral position. *Cell*, *103*(7), 1019-1032.

Simpson, J. H., Kidd, T., Bland, K. S., & Goodman, C. S. (2000). Short-range and long-range guidance by slit and its Robo receptors. Robo and Robo2 play distinct roles in midline guidance. *Neuron*, *28*(3), 753-766.

Stierli, S., Imperatore, V., & Lloyd, A. C. (2019). Schwann cell plasticity-roles in tissue homeostasis, regeneration, and disease. *Glia*. https://doi.org/10.1002/glia.23643

Stierli, S., Napoli, I., White, I. J., Cattin, A. L., Monteza Cabrejos, A., Garcia Calavia, N., Malong, L., Ribeiro, S., Nihouarn, J., Williams, R., Young, K. M., Richardson, W. D., & Lloyd, A. C. (2018). The regulation of the homeostasis and regeneration of peripheral nerve is distinct from the CNS and independent of a stem cell population [Research Support, Non-U.S. Gov't]. *Development*, *145*(24). https://doi.org/10.1242/dev.170316

Tanaka, M., Kuriyama, S., & Aiba, N. (2012). Nm23-H1 regulates contact inhibition of locomotion, which is affected by ephrin-B1. *J Cell Sci*, *125*(Pt 18), 4343-4353. https://doi.org/10.1242/jcs.104083

Theveneau, E., Marchant, L., Kuriyama, S., Gull, M., Moepps, B., Parsons, M., & Mayor, R. (2010). Collective chemotaxis requires contact-dependent cell polarity. *Dev Cell*, *19*(1), 39-53. https://doi.org/10.1016/j.devcel.2010.06.012

Venero Galanternik, M., Kramer, K. L., & Piotrowski, T. (2015). Heparan Sulfate Proteoglycans Regulate Fgf Signaling and Cell Polarity during Collective Cell Migration. *Cell Rep*. https://doi.org/10.1016/j.celrep.2014.12.043

Villar-Cervino, V., Molano-Mazon, M., Catchpole, T., Valdeolmillos, M., Henkemeyer, M., Martinez, L. M., Borrell, V., & Marin, O. (2013). Contact repulsion controls the dispersion and final distribution of Cajal-Retzius cells. *Neuron*, *77*(3), 457-471. https://doi.org/10.1016/j.neuron.2012.11.023

Wang, Y., Teng, H. L., & Huang, Z. H. (2013). Repulsive migration of Schwann cells induced by Slit-2 through Ca2+-dependent RhoA-myosin signaling. *Glia*, *61*(5), 710-723. https://doi.org/10.1002/glia.22464

Worbs, T., Hammerschmidt, S. I., & Forster, R. (2017). Dendritic cell migration in health and disease [Review

Research Support, Non-U.S. Gov't]. *Nat Rev Immunol*, *17*(1), 30-48. https://doi.org/10.1038/nri.2016.116

Yao, M., Qiu, W., Liu, R., Efremov, A. K., Cong, P., Seddiki, R., Payre, M., Lim, C. T., Ladoux, B., Mege, R. M., & Yan, J. (2014). Force-dependent conformational switch of alpha-catenin controls vinculin binding. *Nat Commun*, *5*, 4525. https://doi.org/10.1038/ncomms5525

Ypsilanti, A. R., Zagar, Y., & Chedotal, A. (2010). Moving away from the midline: new developments for Slit and Robo. *Development*, *137*(12), 1939-1952. https://doi.org/10.1242/dev.044511

Zhang, F., Ronca, F., Linhardt, R. J., & Margolis, R. U. (2004). Structural determinants of heparan sulfate interactions with Slit proteins. *Biochem Biophys Res Commun*, *317*(2), 352-357. https://doi.org/10.1016/j.bbrc.2004.03.059

Zochodne, D. W. (2012). The challenges and beauty of peripheral nerve regrowth [Lecture

Research Support, Non-U.S. Gov't]. *J Peripher Nerv Syst*, *17*(1), 1-18. https://doi.org/10.1111/j.1529-8027.2012.00378.x

744

Figure Legends

Figure 1. N-cadherin is required for contact inhibition of locomotion between Schwann cells **a.** Representative still images comparing the collective migration of siRNA Scrambled Control or N-cadherin (N-Cad) KD SCs in a wound healing assay. The dashed lines indicated the leading edge of migration at 0h and 6h. Arrows indicate the direction of migration. Zoomed images on the right show Control SCs form a monolayer, whereas N-Cad KD SCs exhibit loss of cell:cell recognition with cells growing on top of each other. Scale bar=100μm. **b**. Quantification of the area of migration of N-Cad knockdown SCs normalised to Controls from **(a)**. Data is presented as mean± SEM and represent three independent experiments. P values were calculated by using a two-tailed unpaired t-test with Welch's correction. **c.** A representative graph of three independent experiments showing the trajectories of Control or N-Cad knockdown cells treated with siRNA1. n= 36 and 35 for Control and N-Cad knockdown cells respectively. **d-e.** Quantification of the directionality ratio **(d)** and the velocity **(e)** from the cells tracked in **(c)**. The red line indicates the mean. P values were calculated using unpaired 2-tailed *t*-tests. **f.** Representative time-lapse images of a CIL assay, showing control or N-Cad knockdown cells, treated with siRNA1 or siRNA2 that repulsed or overlapped respectively (arrowheads) (Video 1). The blue and green dots indicate the two interacting cells. Arrows indicate the direction of migration. Scale bar=100μm. **g.** Quantification of (**f).** Data are representative of n=3 independent experiments and presented as mean ± SEM. P values were calculated using a two-way ANOVA followed by Sidaks' test for multiple comparisons. *p<0.05, **p<0.01, ***p<0.001. Note, that random protrusions and retractions are produced by SCs in all directions that leads to a high number of apparent repulsion events, even when loss of CIL has occurred. **h.** siRNA Scrambled cells exhibit a change in direction following contact (orange dots) compared to free moving controls, indicative of CIL. N-cadherin knockdown (white dots) results in loss of CIL, with no difference in the displacement index between free moving or N-Cad knockdown cells. ***p<0.001

Figure 2. N-cadherin dependent CIL is independent of the adherens junction complex

a. Representative time-lapse microscopy images of a CIL assay in which red fluorescence-labelled Control cells (C1 and C2) were mixed with green fluorescent-labelled N-cadherin (N-Cad) knockdown cells (N1 and N2) (Video 2). Cells of interest are indicated with a red or green dot for Control and N-Cad knockdown cells, respectively. Arrows indicate the direction of migration. Scale bar=100μm. **b.** Quantification of **(a)** n=3 independent experiments. Graph represents the response of the cell being tracked (in bold) when it encounters the other cell type (not bold). Graph represents mean ± SEM; p values were calculated using a 2-way ANOVA followed by Sidaks test for multiple comparisons. **c.** Schematic illustrating the mixing experiment in **a-b**. When a siRNA Scrambled control encounters another control cell, both cells express N-cad and are repulsed away from each other. When a Control cell makes contact with a N-cad knockdown cell, only the Control cell expressing N-cad is capable of enacting a repulsive signal. **d.** Quantification of the collective migration assay shown in Supplementary Fig 2a, showing the distance migrated upon contact of Control, N-Cad knockdown or Control and N-Cad knockdown cells following release from dual-chamber inserts. Data is presented as mean ± SEM and represents n=3 independent experiments. P values were calculated by a one-way ANOVA followed by Tukey's test for multiple comparisons. **e.** Quantification of CIL in Control and α-catenin knockdown cells. Data is presented as mean ± SEM from three independent experiments. P values were calculated by a one-way ANOVA followed by Tukey's multiple comparisons test. **f.** Quantification of the velocity of Control and α-catenin knockdown cells. Red line indicates mean of n=3 independent experiments. P values were calculated by a two-tailed unpaired *t*-test. **g.** Graph shows the quantification of CIL from n=3 independent experiments. Data is presented as mean ± SEM. P values were calculated by a one-way ANOVA followed by Tukey's multiple comparisons test. **h.** Velocity of the tracks from Control-treated cells (dots) and p120-catenin knockdown cells treated with siRNA1 (squares) or siRNA2 (triangles). Red lines indicate the mean of n=3 independent experiments. P values were calculated by a one-way ANOVA followed by Dunnett's post-test. *$p<0.05$, **$p<0.01$, ***$p<0.001$.

797
798

Figure 3. The extracellular domain of N-cadherin is sufficient to mediate CIL

a. Schematic of N-Cadherin (N-Cad) full length, extracellular and intracellular domains tagged with Tomato at the C-terminus. The intracellular domain of N-Cad has an additional Lyn membrane-targeting sequence at the N-terminus to target it to the membrane. **b.** Representative Western blot using antibodies that recognise the C-terminus of N-Cad and Tomato, showing the expression levels of the constructs, 48 hours after knockdown of endogenous N-Cad using siRNA1. ERK was used a loading control. **c.** Representative time-lapse microscopy images from a CIL assay of N-Cad knockdown cells transfected with siRNA resistant full-length, intracellular domain (siRNA1+ICD) or the extracellular domain (siRNA1+ECD) of N-Cad tagged with Tomato. Arrows indicate the direction of migration. Black arrowheads indicate repulsion events (siRNA1+ full length and ECD). White arrowheads indicate overlapping events (siRNA1 + Full length, ICD and ECD) (Video 3). Cells of interest that are interacting are indicated by blue, red, and green dots. Scale bar=100μm. **d.** Quantification of **(c)** Full length (n=3), the ECD and ICD of N-Cad (n=4) and Control and siRNA1 to N-Cad (n=7). Graph shows the mean±SEM. P values were calculated using a two-way ANOVA followed by Sidaks' test for multiple comparisons, **p<0.01, ***p<0.001.

Figure 4. Glypican-4 and Slit2/Slit3 are required for CIL

a. Quantification of a CIL assay, showing Control or Glypican-4 knockdown cells, treated with siRNA1 or siRNA2, that are repulsed or not repulsed upon contact respectively (Video 4). Data represents n=3 independent experiments and mean ± SEM. P values were calculated using a two-way ANOVA followed by Sidaks multiple comparisons test. **b.** Representative confocal images showing Control or Glypican-4 knockdown cells stained with phalloidin (red) and immunolabelled to detect N-cadherin (N-Cad) (green). Scale bar=50μM. Arrowheads indicate N-cadherin junctions. **c.** Quantification of cluster formation in Control or Glypican-4 knockdown SCs at 72 hours post-knockdown. Data represents n=3 independent experiments and shows mean ± SEM. P values were calculated by a two-way ANOVA followed by the appropriate post-test. **d**. Quantification of CIL in Control or Slit2/Slit3 knockdown cells treated with siRNA1 (n=3, mean ± SEM) (Video 5). P values were calculated using a two-way ANOVA followed by Tukey's post-test for multiple comparisons. **e.** Representative immunofluorescence images of Control and Slit2/3 knockdown SCs stained with phalloidin (red) and N-Cad (green). Scale bar=50μM. Arrowheads indicate N-cadherin junctions. **f.** Quantification o of SCs in clusters in Control or Slit2/Slit3 knockdown cells (n=3, mean ± SEM). P values were calculated using a two-way ANOVA followed by Tukey's test for multiple comparisons. **g.** Representative confocal images showing Control, Robo1 or Robo2 knockdown cells stained with phalloidin (red) and immunolabelled to detect N-cadherin (N-Cad) (green). Scale bar=50μm. Arrowheads indicate N-cadherin junctions **h** Quantification of the percentage of SCs in clusters following Control or Robo1 or Robo2 knockdown (n=3, mean ± SEM). P values were calculated using a two-way ANOVA followed by Tukey's test for multiple comparisons. **i.** Representative confocal images from n=3 independent experiments of Sox2 overexpressing SCs compared to Slit2/Slit3 knockdown SCs stained with phalloidin to detect F-actin (red), antibodies to detect N-Cad (green) and Hoechst to detect nuclei (blue). Scale bar=50μm. *p<0.05, **p<0.01, ***p<0.001.

Figure 5. N-cadherin is required for the trafficking of Slit2/Slit3 to the cell-surface

a-d. Representative confocal images of Control or N-cadherin (N-Cad) knockdown SCs. Cells were labelled with antibodies to **(a)** Slit2 or **(c)** Slit3 (green) with quantification of Slit2 and Slit3 levels in the cell protrusions indicated by the boxes (n=3, mean±SEM for both conditions). Scale bar=15μm. P values were calculated by a one-way ANOVA followed by Tukey's multiple comparisons tests. **e.** Representative confocal images of rescue experiments in which SCs depleted of N-Cad were transfected with the N-Cad ECD tagged with Tomato, or Tomato Control Vector and immunolabelled to detect Slit2 (green). Scale bar=15μm **f.** Quantification of **(e)** (n=3, mean ±SEM). P values were calculated by a one-way ANOVA followed by Tukey's multiple comparisons tests. **g.** As **(e)** but stained for Slit3 (green). **h.** Quantification of **(g)** (n=3, mean ±SEM). Scale bar=15μm. P values were calculated by a one-way ANOVA followed by Tukey's multiple comparisons tests. *$p<0.05$, **$p<0.01$.

Figure 6. The Slit repulsive signal is required for the efficient collective migration of Schwann cells during nerve regeneration

a. Quantification of the collective migration of Control compared to Slit2/Slit3 knockdown SCs at 6 hours using a chamber assay (Video 7). Data is normalised to Control and presented as mean area±SEM of n=3 independent experiments. P values were calculated by an unpaired two-tailed *t*-test with Welch's correction, compared to control. **b**. Representative confocal images of SCs treated with recombinant-Slit2 (rSlit2) or PBS immunolabelled to detect N-Cadherin (N-Cad) (green) and co-stained with phalloidin (red) to detect F-actin and Hoechst to detect nuclei (blue). (n=3) Scale=50μM. **c**. Quantification of SC clusters from **(b)** (n=3, mean±SEM) (Video 8). P values were calculated using a two-way ANOVA followed by Sidaks test for multiple comparisons. **d.** Graph shows the collective migration of SCs in a chamber assay treated with rSlit2 or PBS control (n=3, mean area±SEM). P values were calculated by an unpaired two-tailed *t*-test with Welch's correction, compared to PBS controls. **e**. Graph shows the Euclidean distance (shortest distance travelled) for cells in **(d)** at 24 hours (PBS n=141 rSlit2 n=138 from n=3 independent experiments). The red line denotes the mean. P values were calculated by an unpaired two-tailed *t*-test. **f.** Graph shows tracks of individual cells in the collective migration assay quantified in **(d)** n=3. **g.** Representative confocal images of Sox2-induced SC clusters treated with Shield for 24 hours and PBS or rSlit2 immunolabelled to detect N-Cad (green) and co-stained with phalloidin (red) to detect F-actin and Hoechst to detect nuclei (blue) (Video 9). Scale bar=50μM. **h.** Quantification of cell roundness of Sox2-induced SC clusters treated with PBS or rSlit2. (n=3, mean±SEM). Data was normalised to Sox2 controls and p values calculated using an unpaired two-tailed *t*-test. **i.** Polar histograms showing alignment of nuclei within each cluster from PBS (n=168) or rSlit2 (n=166) treated Sox2 SCs as an indicator of polarisation. Angles closer to 0 represent more aligned nuclei in the PBS (blue) whereas they are more randomly distributed in the rSlit2 treated Sox2 SCs (orange). Data is representative of n=3. **j.** Representative confocal images of Sox2 SC clusters treated with Control, or Slit2/Slit3 siRNAs and immunolabelled to detect N-Cad (green) and co-stained with phalloidin (red) to detect F-actin and Hoechst to detect nuclei

884 (blue). Scale bar=50μm. **k.** Quantification of the cell roundness of individual cells in Sox2-induced
885 SC clusters treated with Control or Slit2/Slit3 siRNA1 or 2. (n=3, mean±SEM). Data was
886 normalised to Sox2 controls and p values calculated using an unpaired two-tailed *t*-test. **l.**
887 Schematic illustrating that in control conditions SC exhibit CIL but upon KD of N-cadherin, CIL
888 is lost and SCs become invasive. Knockdown or inhibition of Slit2/Slit3 inhibits CIL but the
889 peristence of N-cadherin expression results in the formation of non-migratory clusters. In contrast,
890 SC cords in which Sox2 is activated, maintain CIL signals which drive their collective migration.
891 *p<0.05 **p<0.01, ***p<0.001.
892

Figure 7. The Slit repulsive signal is required for the efficient collective migration of Schwann cells in the ex vivo nerve bridge

a. Schematic showing ex vivo migration protocol. **b.** Representative immunofluorescence images in untreated ex vivo explants showing plp-eGFP SCs (green) migrating along the vasculature (magenta) in the ex vivo bridge. Arrowheads indicate SCs in close contact with blood vessels. Scale bar=100 μm. **c.** Representative tile scan images of the nerve bridge explants following nerve transection in plp-eGFP (green) mice at 24h after treatment with PBS or rSlit (40μg/ml). At 24h PBS treated explants showed the migration of polarised cords of SC into the bridge. In contrast, rSlit2 treated sections showed less SC migration, with groups of clustered, more round cells. Scale bar=100 μm. **d.** Graph showing quantification of SC migration at 24h following treatment with either PBS or rSlit2 in tile scan images. Data was expressed as the fold change in migration from 0h. Data are representative of n=9 animals/group from n=5 independent experiments. Data are represented as mean area±SEM and P values calculated by an unpaired two-tailed *t*-test. **e.** Representative ex vivo images of the nerve bridge 24h following treatment with PBS or rSlit2 to detect SC with endogenous plp-eGFP (green) and Hoechst (blue). Images show that PBS SC appear to migrate as directional cords whereas rSlit2 treated SC exhibit a rounder and more clustered phenotype (Video 10). Scale bar=50μm. Images are representative of n=4 animals/group from n=3 independent experiments. **f.** Quantification of **d.** comparing the number of SC in cords following PBS or rSlit2 treatment and expressed as a percentage. P values calculated by a Fisher's exact test (n=4 animals/group mean±SEM). **g.** Quantification of **d.** showing the number of SC in clusters following PBS or rSlit2 treatment and expressed as a percentage**.** (n=4 animals/group mean±SEM). P values calculated by a Fisher's exact test. **h.** Representative 3D surface reconstructed images of nerve bridge explants following PBS or rSlit2 treatment labelled for SC (plp-eGFP, green), Nuclei (blue) and SC nuclei (white). Images were used to quantify the sphericity of the migrating SC. **i.** Quantification of SC roundness from (h). PBS (n=64), rSlit2 (n=65). P values were calculated by an unpaired *t*-test with Welch's correction, n=4 animals/group mean±SEM (red). **j.** Quantification of nuclear alignment of SCs to the leader cell within a cord or

cluster. PBS (n=41) rSlit (n=40) P values were calculated by an unpaired *t*-test with Welch's correction, n=3 animals/group mean±SEM. **k.** Quantification SC persistent migration. Graph represents how far SC groups have deviated from directed migration into the bridge. PBS (n=72) rSlit (n=71) P values were calculated by an unpaired *t*-test with Welch's correction, n=4 animals/group mean±SEM (red). **l.** Cartoon representing the dual role of N-cadherin in SC collective migration. *p<0.05, **p<0.01, ***p<0.001.

Supplementary Figure Legends

Figure 1-figure supplement 1. N-cadherin is required for contact inhibition of locomotion between Schwann cells

a. Representative Western blot from 3 independent experiments showing N-cadherin (N-Cad) protein levels in SCs treated with either 2nM control, siRNA1 or siRNA2 for 48 hours. ERK was used as a loading control. **b.** Representative confocal images of Control, siRNA1 or siRNA2 treated cells at 36 hours, immunostained to detect N-Cad (green), F-actin (red) and nuclei were labelled with Hoechst (blue). White arrows indicate the cell contacts. Images are representative of n=3 experiments. Scale bar=20μm. **c.** Representative bright-field images of SCs, or N-cad siRNA1 or siRNA2. Note that whereas Control SCs form a monolayer, N-cad siRNA-treated cells grow on top of each other. Images are representative of n=3 independent experiments. Scale bar=200μm.

Figure 2-figure supplement 1. N-cadherin dependent CIL is independent of the adherens junction complex

a. Representative images from time-lapse microscopy showing the collective migration of Control, N-cadherin (N-Cad) knockdown or Control and N-Cad knockdown SCs upon contact and at 24h following the removal of inserts in a dual-chamber assay in which SCs on the right are labelled with CellTracker (green). Dashed lines in the upper panels indicate the initial contact of the migrating cells, and in the lower panel indicate the leading edge of migrating cells at 24 hours. Arrows indicate the direction of migration. Images on the right show phase-contrast images showing mixing (upper) or boundary (lower) formation upon cell contact. **b.** Representative confocal images of Control-treated and α-catenin knockdown cells at 36 hours, immunostained to detect α-catenin (blue), N-Cad (green) and co-stained for F-actin (red). Note N-Cad is still localised at the junctions following alpha catenin knockdown (arrowheads) but actin is no longer polarised at these junctions. Scale bar=20μm. **c.** Representative Western blots showing the efficiency of (**c**) α-catenin or (**e**) p120-catenin knockdown using two independent siRNAs compared to Control at 36 hours for α-catenin and at 96 hours for p120-catenin. ERK was used as a loading control. **d.** Representative confocal images of Control or p120-catenin knockdown cells at 96 hours, immunostained for N-Cad (green), and co-stained for F-actin (red) and nuclei (blue). Arrowheads indicate N-Cad positive cell-contacts. Scale bar=20μm. All data are representative of n=3 independent experiments.

Figure 3- figure supplement 1. The extracellular domain of N-cadherin is sufficient to mediate CIL

a. Representative confocal images of N-Cadherin (N-cad) knockdown cells overexpressing siRNA-resistant, Tomato-tagged N-Cad full length (left panel), the intracellular domain (middle panel), or the extracellular domain of N-Cad (right panel) (red), immunolabelled to detect p120-catenin (green) or α-catenin (blue). Enlarged images show cell-contact points indicated by white rectangles. Images are representative of n=3 independent experiments. Scale bar=20μm.

Figure 4- figure supplement 1. Glypican-4 and Slit2/Slit3 are required for CIL

a. Quantification of CIL in Control or EphB2 knockdown SCs. (n=3, mean±SEM). P values were calculated by a two-way ANOVA followed by Sidaks test for multiple comparisons. **b.** Graph shows Glypican-4 mRNA levels detected by RT-qPCR of Control or Glypican-4 knockdown SCs at 36 hours (n=3, mean±SEM). **c.** Quantification of the velocity of individual cells in **Figure 4a**, red line shows the mean, n=30 cells/ group from n=3 independent experiments. P values were calculated using a one-way ANOVA followed by multiple comparisons test. **d.** Quantification of number of overlapping cells per field of view in N-cadherin (N-cad), Glypican-4 or N-cad + Glypican-4 knockdown cells (n=3, mean±SEM). P values calculated by one-way ANOVA followed by multiple comparisons test. **e.** Representative confocal images from **d.** Arrow heads indicate junctions, arrows indicate overlapping cells. scale bar=10μm. **f.** Representative gel showing the expression of the different Slit ligand and Robo receptors in SCs as detected by RT-qPCR (n=3). **g.** Representative Western blots of Control and Slit2/Slit3 knockdown cells from n=3 independent experiments, showing the knockdown efficiency and N-cadherin (N-Cad) expression levels. Vinculin was used as a loading control. **h.** Graph shows Robo1 and Robo2 mRNA levels detected by RT-qPCR of Control or Robo1 and Robo2 knockdown SCs at 36 hours (n=3, mean±SEM). **i.** Quantification of cell roundness in SCs overexpressing Sox2 compared to Slit2/Slit3 KD in control SC normalised to Sox2 SCs. Data is representative of n=3 independent experiments. P values were caluclated using a one-way ANOVA followed by Sidaks test for multple comparisons *$p<0.05$ ***$p<0.001$.

Figure 5 -figure supplement 1. N-cadherin is required for the localisation of Slit2/Slit3 at the cell surface.

a. Representative Western blot (n=3) of Control and N-cadherin (N-Cad) knockdown cells, probed for Slit2, Slit3 and N-Cad. Vinculin was used as a loading control. **b.** Graph showing mRNA expression levels of Slit2, Slit3 and Glypican-4 in N-Cad knockdown cells compared to Control (mean±SEM, from n=3 independent experiments). **c.** Representative Western blot showing the co-immunoprecipitation of either Tomato or full-length N-Cad tagged with Tomato, co-expressed with myc-tagged Slit2 in HEK cells. Blots were probed with anti-tomato, anti-myc and anti-Slit2 antibodies. (n=3). **d.** Representative stills from spinning disc confocal images of SCs transfected with Tomato labelled N-Cad, demonstrating the dynamic activity of N-Cad (red) arriving at waves towards the moving front of cells (see Video 6). Arrowheads indicate N-Cad at cell-cell contacts. Arrows indicate waves of N-Cad moving towards the front of the lamellipodia of SCs. Scale bar=50μm. **e.** Quantification of total Slit2 and **f.** Slit3 intensity in N-Cad KD cells compared to Control (each dot represents a single cell from n=3, red bars represent mean±SEM). P values were calculated by unpaired t-test. **g.** Representative immunofluorescence images of Slit2 (white) and Slit3 (white) staining following N-cad knockdown. Note the lack of Slit2/3 staining at the cell protrusions, but with expression detectable in the perinuclear area. Dashed lines denote outline of cell. Scale bar=10μm **h.** Representative immunofluorescence images of Slit2 (white) staining at the membrane in Free Moving and cells in Contact. Arrow heads indicate Slit2 (white) staining at the membrane and arrowheads indicate Slit2 staining at the site of contact. Scale bar=10μm **i.** Representative immunofluorescence images of Slit2 staining at the membrane in Control and Glypican-4 KD cells. Scale bar=10μm **p<0.01. n.s=not significant.

Figure 6-figure supplement 1. The Slit repulsive signal is required for the efficient collective migration of Schwann cells

a. Representative stills from time-lapse microscopy (Video 7) showing the collective migration of Control or Slit2/Slit3 knockdown SCs seeded in chambers at the indicated time-points and quantified in **Figure 6a**. (n=3). The dashed lines indicate the leading edge of the migrating cells. Arrows indicate the direction of migration. Scale bar=50μm. **b.** As in (**a**) but the SCs were treated with 2μg/ml recombinant-Slit-2 (rSlit2) or PBS (n=3), quantified in **Figure 6d.** (Video 9) Scale bar=50 μm. **c.** Representative Western blot showing pTuner empty vector SCs or pTuner Sox2 SCs response to Shield treatment at 24 hours. Note that high Sox2 expression is only evident in the Shield treated pTuner Sox2 SCs at 24 hours. **d.** Diagram showing how nuclear alignment and cluster roundness were quantified **e.** Quantification of overall cluster roundness in Sox2 SCs treated with rSlit2 or **f.** Slit2/3 siRNA (each dot represents a cluster from n=3, red bars represent mean±SEM). **g.** Polar histograms representative of n=3 experiments, showing the alignment of the nuclei within each cluster in Control (blue) or Slit2/3 siRNA 1 and Slit2/3 siRNA2 (orange). P values were calculated by t-test or one-way ANOVA as appropriate **p<0.01, ***p<0.001.

Figure 7-figure supplement 1. The Slit repulsive signal is required for the efficient collective migration of Schwann cells ex vivo

a. Representative tile scans of untreated ex vivo explants showing the components of the bridge. Images show densely packed nuclei (blue) between the proximal and distal stumps. Regrowing axons (white) are evident following the SC (green) cords, which are migrating along the **b.** vasculature (red). Scale bars=100μm. **c.** Representative tile scan images from ex vivo explants harvested on Day 5 following sciatic nerve injury at 0h and 24 hours following treatment with PBS or rSlit2 (40μg/ml) and quantified in **Fig 7b**. Images show similar levels of SC migration into the bridge between groups at the 0h time point as marked by plp-eGFP (green). At 24h post treatment, rSlit2 treated nerves show reduced SC migration into the bridge. Images are representative of n=9 animals/group from n=3 independent experiments. Dashed lines indicate area where migration begins. Scale bar=100μm. **d.** Imaris diagram showing quantification of SC persistence of migration ex vivo. **(i)** The angle of SC cords was measured relative to the stump. **(ii)** The angle of each nucleus within a cord was measured and compared to the leader cell and expressed as SC alignment to leader (degrees).

Video Legends

Figure 1-Video 1. N-cadherin mediates contact inhibition of locomotion (CIL)

Related to Figure 1f. Representative time-lapse microscopy of Control and N-cadherin (N-Cad) knockdown Schwann cells treated with siRNA1 or siRNA2, that repulsed or overlapped respectively. Cells of interest are indicated with a green and blue dot.

Figure 2-Video 1. CIL is independent of *trans*-homodimerisation

Related to Figure 2a. Representative time-lapse microscopy of a CIL assay in which red-labelled Control cells were mixed with green-labelled N-cadherin (N-Cad) knockdown cells. Cells of interest are indicated with a red or green dot for Control and N-Cad knockdown cells, respectively.

Figure 3-Video 3. The Extracellular domain is sufficient to mediate CIL

Related to Figure 3c. A video compilation of representative time-lapse microscopy from a CIL assay of N-cadherin (N-Cad) knockdown cells transfected with the full-length of N-Cad (siRNA1+FL), the intracellular domain of N-Cad (siRNA1+ICD) or the extracellular domain of N-Cad (siRNA1+ECD) tagged with Tomato. Cells of interest that are interacting are indicated by blue, red, and green dots.

Figure 4-Video 1. Glypican-4 is required for CIL between Schwann cells

Related to Figure 4a. Representative time-lapse microscopy of a CIL assay, showing Control or Glypican-4 knockdown cells, treated with siRNA1 (si1) or siRNA2 (si2), that are repulsed or not repulsed upon contact respectively. The green and blue dots indicate the interacting cells.

Figure 4-Video 2. Slit2/3 mediates CIL between Schwann cells

Related to Figure 4h. Representative time-lapse microscopy of showing Sox2 overexpressing or Slit2/3 knockdown cells, treated with siRNA1. Sox2 induces SC clustering of migratory, polarised cords, in which the CIL signal is maintained. In contrast, Slit2/3 knockdown in SCs results in quieter, more round clusters.

Figure 5-Video 1. N-cadherin moves in waves towards cell contacts

Related to Supplementary Figure 5d. Spinning disc confocal microscopy of SCs transfected with construct expressing siRNA resistant tomato-tagged N-cadherin in order to visualise N-Cad movement during cell migration. This video demonstrates the dynamic activity of N-Cad which arrives in waves towards the moving front of the cell.

Figure 6-Video 1. Slit2/3 are required for the efficient collective migration of Schwann cells

Related to Figure 6a. Representative time-lapse microscopy of the collective migration of Schwann cells (SCs) treated with Control siRNA or Slit2/3 siRNA2. Following Slit2/3 knockdown, SCs are clustered and migrate less efficiently towards to gap.

Figure 6-Video 2. Recombinant Slit2 induces Schwann cell Clustering

Related to Figure 6c. Representative time-lapse microscopy of a cell clustering assay, showing PBS or recombinant Slit2 (rSlit2)-treated Schwann cells, that are repulsed and not repulsed upon contact respectively.

Figure 6-Video 3. Slit2 is required for the efficient collective migration of Schwann cells

Related to Figure 6d. Representative time-lapse microscopy of a collective migration assay, showing PBS or recombinant Slit2 (rSlit2)-treated Schwann cells (SCs). Note, rSlit2-treated SCs close the gap more slowly than PBS treated cells.

Figure 7-Video 1. Slit2 is required for the collective migration of Schwann Cells within a regenerating nerve

Related to Figure 7b. Representative time lapse microscopy of nerve explants from mice 5 days following sciatic nerve transection showing the effect of PBS or recombinant Slit2 (rSlit2) (60μg/ml) treatment on migration into the nerve bridge. PBS treated explants migrated in cords, whereas SC in nerves treated with rSlit2 became clustered.

Source Data Legends

Figure 1-Source Data 1 Original file for the Western blot analysis of N-cadherin KD in Figure 1figure supplement 1 a (N-cadherin)

Figure 1-Source Data 2 Labeled file for the Western blot analysis of N-cadherin KD in Figure 1figure supplement 1 a (N-cadherin)

Figure 1-Source Data 3 Original file for the Western blot analysis of loading control in Figure 1figure supplement 1 a (ERK)

Figure 1-Source Data 4 Labelled file for the Western blot analysis of loading control in Figure 1figure supplement 1 a (ERK)

Figure 2-Source Data 1 Original file for the Western blot analysis of alpha catenin KD in Figure 2figure supplement 1 c (alpha catenin)

Figure 2-Source Data 2 Labelled file for the Western blot analysis of alpha catenin KD in Figure 2figure supplement 1 c (alpha catenin)

Figure 2-Source Data 3 Original file for the Western blot analysis of loading control in Figure 2figure supplement 1 c (ERK)

Figure 2-Source Data 4 Labelled file for the Western blot analysis of loading control in Figure 2figure supplement 1 c (ERK)

Figure 2-Source Data 5 Original file for the Western blot analysis of p120 catenin KD in Figure 2figure supplement 1 e (p120 catenin)

Figure 2-Source Data 6 Labelled file for the Western blot analysis of p120 catenin KD in Figure 2figure supplement 1 e (p120 catenin)

Figure 2-Source Data 7 Original file for the Western blot analysis of N-cadherin in Figure 2figure supplement 1 e (N-cadherin)

Figure 2-Source Data 8 Labelled file for the Western blot analysis of N-cadherin in Figure 2figure supplement 1 e (N-cadherin)

Figure 2-Source Data 9 Original file for the Western blot analysis of loading control in Figure 2figure supplement 1 e (ERK)

Figure 2-Source Data 10 Labelled file for the Western blot analysis of loading control in Figure 2figure supplement 1 e (ERK)

Figure 3-Source Data 1 Original file for the Western blot analysis of N-cadherin KD in Figure 3b (N-cadherin)

Figure 3-Source Data 2 Labelled file for the Western blot analysis of N-cadherin KD in Figure 3b (N-cadherin)

Figure 3-Source Data 3 Original file for the Western blot analysis showing the expression levels of the constructs in Figure 3b (Tomato)

Figure 3-Source Data 4 Labelled file for the Western blot analysis showing the expression levels of the constructs in Figure 3b (Tomato)

Figure 3-Source Data 5 Original file for the Western blot analysis of loading control in Figure 3b (ERK)

Figure 3-Source Data 6 Original file for the Western blot analysis loading control in Figure 3b (ERK)

Figure 4-Source Data 1 Original gel for analysis of Robo1-3 expression in SCs in Figure 4figure supplement 1f

Figure 4-Source Data 2 Labelled gel for analysis of Robo1-3 expression in SCs in Figure 4figure supplement 1f

Figure 4-Source Data 3 Original gel for analysis of Robo 4 expression in SCs in Figure 4figure supplement 1f

Figure 4-Source Data 4 Labelled gel for analysis of Robo 4 expression in SCs in Figure 4figure supplement 1f

Figure 4-Source Data 5 Original file for the Western blot analysis of Slit2/3 KD in Figure 4figure supplement 1g (Slit2)

Figure 4-Source Data 6 Labelled file for the Western blot analysis of Slit2/3 KD in Figure 4figure supplement 1g (Slit2)

Figure 4-Source Data 7 Original file for the Western blot analysis of Slit2/3 KD in Figure 4figure supplement 1g (Slit3)

Figure 4-Source Data 8 Labelled file for the Western blot analysis of Slit2/3 KD in Figure 4figure supplement 1g (Slit3)

Figure 4-Source Data 9 Original file for the Western blot analysis of Slit2/3 KD in Figure 4figure supplement 1g (N-cadherin)

Figure 2-Source Data 10 Labelled file for the Western blot analysis of Slit2/3 KD in Figure 4figure supplement 1g (N-cadherin)

Figure 4-Source Data 11 Original file for the Western blot analysis of loading control in Figure 4figure supplement 1g (Vinculin)

Figure 4-Source Data 12 Labelled file for the Western blot analysis of loading control in Figure 4figure supplement 1 g (Vinculin)

Figure 5-Source Data 1 Original file for the Western blot analysis of N-cadherin KD in Figure 5figure supplement 1a (N-Cadherin)

Figure 5-Source Data 2 Labelled file for the Western blot analysis of N-cadherin KD in Figure 5figure supplement 1a (N-cadherin)

Figure 5-Source Data 3 Original file for the Western blot analysis of N-cadherin KD in Figure 5figure supplement 1a (Slit2)

Figure 5-Source Data 4 Labelled file for the Western blot analysis of N-cadherin KD in Figure 5figure supplement 1a (Slit2)

Figure 5-Source Data 5 Original file for the Western blot analysis of N-cadherin KD in Figure 5figure supplement 1a (Slit3)

Figure 5-Source Data 6 Labelled file for the Western blot analysis of N-cadherin KD in Figure 5figure supplement 1a (Slit3)

Figure 5-Source Data 7 Original file for the Western blot analysis of N-cadherin KD in Figure 5figure supplement 1a (Vinculin)

Figure 5-Source Data 8 Labelled file for the Western blot analysis of N-cadherin KD in Figure 5figure supplement 1a (Vinculin)

Figure 5-Source Data 9 Original file for the Western blot showing the co-immunoprecipitation of either Tomato or full-length N-Cad tagged with Tomato, co-expressed with myc-tagged Slit2 in HEK cells in Figure 5figure supplement 1c (Slit2)

Figure 5-Source Data 10 Labelled file for the Western blot showing the co-immunoprecipitation of either Tomato or full-length N-Cad tagged with Tomato, co-expressed with myc-tagged Slit2 in HEK cells in Figure 5figure supplement 1c (Slit2)

Figure 5-Source Data 11 Original file for the Western blot showing the co-immunoprecipitation of either Tomato or full-length N-Cad tagged with Tomato, co-expressed with myc-tagged Slit2 in HEK cells in Figure 5figure supplement 1c (myc)

Figure 5-Source Data 12 Labelled file for the Western blot showing the co-immunoprecipitation of either Tomato or full-length N-Cad tagged with Tomato, co-expressed with myc-tagged Slit2 in HEK cells in Figure 5figure supplement 1c (myc)

Figure 5-Source Data 13 Original file for the Western blot showing the co-immunoprecipitation of either Tomato or full-length N-Cad tagged with Tomato, co-expressed with myc-tagged Slit2 in HEK cells in Figure 5figure supplement 1c (tomato)

Figure 5-Source Data 14 Labelled file for the Western blot showing the co-immunoprecipitation of either Tomato or full-length N-Cad tagged with Tomato, co-expressed with myc-tagged Slit2 in HEK cells in Figure 5figure supplement 1c (tomato)

Figure 6-Source Data 1 Original gel for analysis of Western blot showing pTuner empty vector SCs or pTuner Sox2 SCs response to Shield treatment at 24 hours in Figure 6figure supplement 1c (N-Cadherin)

Figure 6-Source Data 2 Labelled gel for analysis of Western blot showing pTuner empty vector SCs or pTuner Sox2 SCs response to Shield treatment at 24 hours in Figure 6figure supplement 1c (N-Cadherin)

Figure 6-Source Data 3 Original gel for analysis of Western blot showing pTuner empty vector SCs or pTuner Sox2 SCs response to Shield treatment at 24 hours in Figure 6figure supplement 1c (Sox2)

Figure 6-Source Data 4 Labelled gel for analysis of Western blot showing pTuner empty vector SCs or pTuner Sox2 SCs response to Shield treatment at 24 hours in Figure 6figure supplement 1c (Sox2)

Figure 6-Source Data 5 Original gel for analysis of Western blot showing loading controls for pTuner empty vector SCs or pTuner Sox2 SCs response to Shield treatment at 24 hours in Figure 6figure supplement 1c (Vinculin and alpha tubulin)

Figure 6-Source Data 6 Labelled gel for analysis of Western blot showing loading controls for pTuner empty vector SCs or pTuner Sox2 SCs response to Shield treatment at 24 hours in Figure 6figure supplement 1c (Vinculin and alpha tubulin)

1

Key Resources Table				
Reagent type (species) or resource	**Designation**	**Source or reference**	**Identifiers**	**Additional information**
Other	Plp-eGFP	(Mallon, 2002)		Available from Jackson Laboratories https://www.jax.org/strain/033357
cell line (rattus norvegius)	Schwann Cells	(Mathon, 2001)	SCs	
cell line (rattus norvegius)	Sox2 Schwann Cells	This paper		Created using the Proteotuner Shield System by Clontech
cell line (rattus norvegius)	ProteoTuner Schwann Cells	This paper		Created using the Proteotuner Shield System by Clontech
sequence-based reagent	αE-catenin siRNA1	This paper	siRNA	AAGAACGCCTGGAAAG CATAA
sequence-based reagent	αE-catenin siRNA2	This paper	siRNA	CAACCGGGACTTGATAT ACAA
sequence-based reagent	Cadherin-2 siRNA1	This paper	siRNA	TCCCAACATGTTTACAA TCAA
sequence-based reagent	Cadherin-2 siRNA2	This paper	siRNA	CAGTATACGTTAATAATT CAA
sequence-based reagent	p120-catenin siRNA1	This paper	siRNA	AGGTCAGATCGTGGAAA CCTA
sequence-based reagent	p120-catenin siRNA2	This paper	siRNA	ATGCTCGGAACAACAAA GAGTTAA

sequence-based reagent	Glypican-4 siRNA1	This paper	siRNA	CCGACTGGTTACTGATGTCAA
sequence-based reagent	Glypican-4 siRNA2	This paper	siRNA	CGGTGTAGTTACAGAACTGTA
sequence-based reagent	Slit2 siRNA1	This paper	siRNA	ATCAATATTGATGATTGCGAA
sequence-based reagent	Slit2 siRNA1	This paper	siRNA	GACGACTAGACCGTAGTAATA
sequence-based reagent	Slit3 siRNA1	This paper	siRNA	AACGGCGGTGCCCAAAGAATT
sequence-based reagent	Slit3 siRNA1	This paper	siRNA	ATCGTGGAAATACGCCTAGAA
sequence-based reagent	Robo1 siRNA1	This paper	siRNA	AAGGGCGGCGAAAGAGTGGAA
sequence-based reagent	Robo1 siRNA2	This paper	siRNA	CCCGACTATAGAATGGTACAA
sequence-based reagent	Robo2 siRNA1	This paper	siRNA	CTCATTGGATTGTCCGGCTAA
sequence-based reagent	Robo2 siRNA2	This paper	siRNA	CTCGGACACTATCCTGCGGAA
sequence-based reagent	N-cadherin siRNA1 targeting sequence	This paper	Forward Primer	5'-CACGATAAACAATGAGACTGGGGACATC-3'
sequence-based reagent	N-cadherin siRNA1 targeting sequence	This paper	Reverse Primer	Reverse primer 5'-AACATATTGGGTGAAGGTGTGCTGGG-3'
sequence-based reagent	Slit1 Forward	This paper	PCR primers	GCACTTGTCACAATGACCCT

sequence-based reagent	Slit1 Reverse	This paper	PCR primers	CCCTTCAAAGCCGGAAGGA
sequence-based reagent	Slit2 Forward	This paper	PCR primers	GTGTTAGAAGCCACGGGAAT
sequence-based reagent	Slit2 Reverse	This paper	PCR primers	GCGTCTGGTGTGAATGAGAT
sequence-based reagent	Slit3 Forward	This paper	PCR primers	GGATTATCGCAACAGATTCAG
sequence-based reagent	Slit3 Reverse	This paper	PCR primers	GGTCAGTGGTATATTCAGGG
sequence-based reagent	Robo1 Forward	This paper	PCR primers	AGGGGAGTCAGAATCTGCTT
sequence-based reagent	Robo1 Reverse	This paper	PCR primers	CCTCTGGACGTTCGTAACAG
sequence-based reagent	Robo2 Forward	This paper	PCR primers	TTGGATCAGAGGAGTCCCTG
sequence-based reagent	Robo2 Reverse	This paper	PCR primers	ACCCTTTAGAGGAGGCTGTT
antibody	N-Cadherin (mouse, monoclonal)	BD Transduction	610920	1:1000 Immunofluorecence Western Blot
antibody	α-catenin (rabbit, polyclonal)	Sigma	C2081	1:1000 Immunofluorecence Western Blot
antibody	β-catenin (mouse, monoclonal)	BD transductions	610920	1:2000 Immunofluorecence Western Blot
antibody	p120-catenin (mouse, monoclonal)	BD Transduction	61034	1:2000 Immunofluorecence Western Blot

antibody	ERK1/2 (rabbit, polyclonal)	Sigma	M5670	1:1000 Western Blot
antibody	mCherry (rabbit, polyclonal)	Abcam	ab183628	1:1000 Western Blot
antibody	mCherry (rat, monoclonal)	Life technologies	M11217	1:1000 Immunoprecipitation
antibody	Slit2 (rabbit, monoclonal)	Abcam	ab134166	1:1000 Western Blot
antibody	Slit2 (rabbit, polyclonal)	Thermo Fisher Scientific	PA531133	1:1000 Immunofluorescence
Antibody	Slit3 (rabbit, polyclonal)	Sigma	SAB2104337	1:1000 Immunofluorescence
Antibody	Slit3 (Goat, polyclonal)	R&D Systems	AF3629	1:1000 Western Blot
Antibody	Myc (mouse, monoclonal)	Merck Millipore	05-724	1:1000 Western Blot
Antibody	Alexa Fluor 546 Phalloidin	Life technologies	A22283	1:1000 Immunofluorescence
Antibody	Goat anti-Mouse Alexa Fluor 488	Thermo Fisher Scientific	A1100	1:1000 Immunofluorescence
Antibody	Rabbit IgG HRP	GE Healthcare	NA934V	1:1000 Western Blot
Antibody	Mouse IgG HRP	GE Healthcare	NA931V	1:1000 Western Blot
Antibody	Goat IgG HRP	R&D Systems	HAF012	1:1000 Western Blot
software, algorithm	Prism	Graph Pad		https://www.graphpad.com/scientific-software/prism/

software, algorithm	Adobe Photoshop	Adobe Systems		https://www.adobe.com/
software, algorithm	Adobe Illustrator	Adobe Systems		https://www.adobe.com/
software, algorithm	Fiji/ImageJ	{Schindelin, 2012 #370}		https://imagej.net/Fiji/Downloads
software, algorithm	Imaris V9.1.2	Oxford Instruments		https://imaris.oxinst.com/
software, algorithm	Volocity	**Quorum Technologies Inc.**		https://www.volocity4d.com/
software, algorithm	Matlab	MathWorks		

Figure 1.

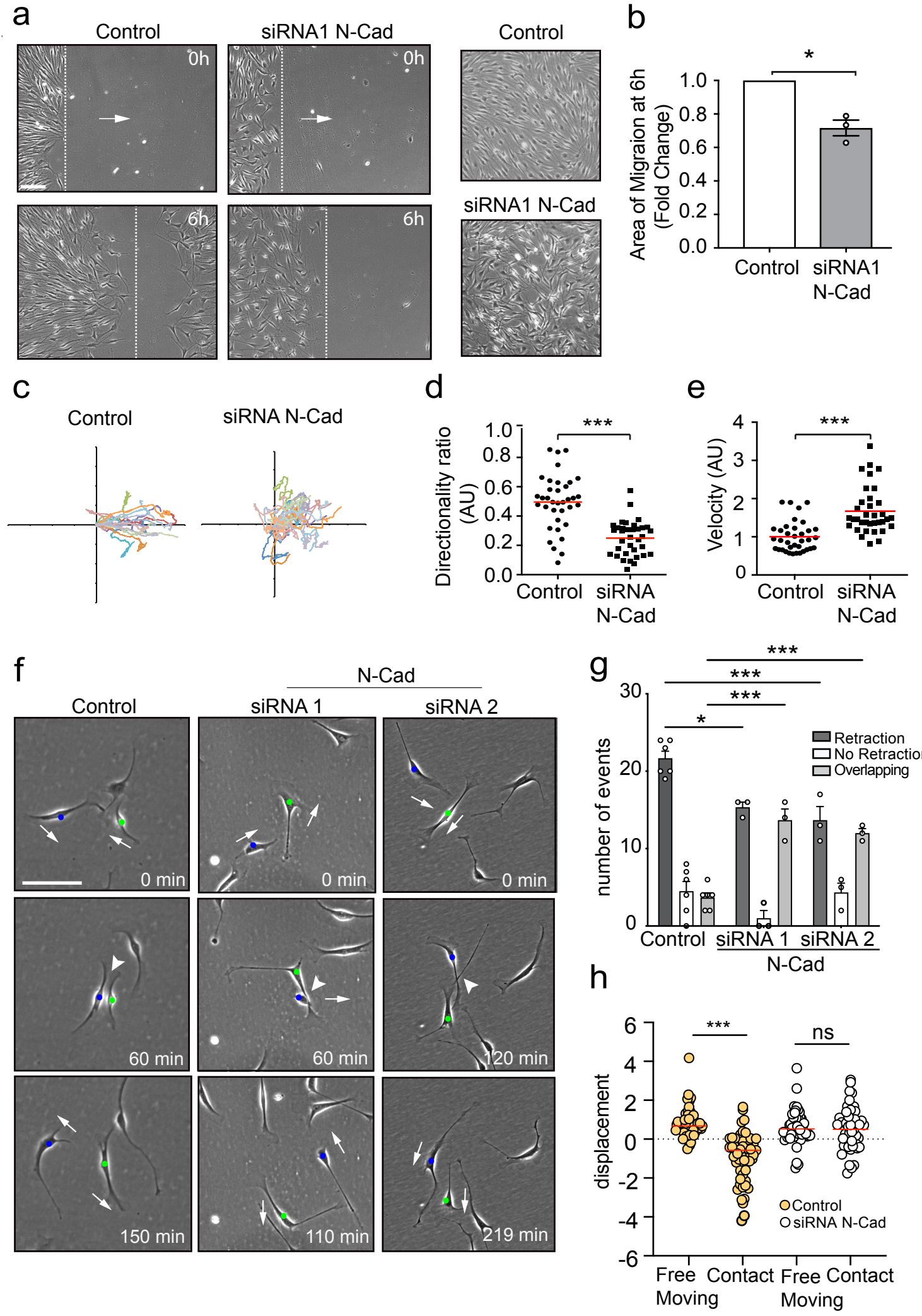
a
Control
siRNA1 N-Cad
Control
0h
0h
6h
6h
siRNA1 N-Cad
b
Area of Migraion at 6h (Fold Change)
1.0
0.8
0.6
0.4
0.2
0.0
*
Control
siRNA1 N-Cad
c
Control
siRNA N-Cad
d
Directionality ratio (AU)
1.0
0.8
0.6
0.4
0.2
0.0
***
Control
siRNA N-Cad
e
Velocity (AU)
4
3
2
1
0
***
Control
siRNA N-Cad
f
N-Cad
Control
siRNA 1
siRNA 2
0 min
0 min
0 min
60 min
60 min
120 min
150 min
110 min
219 min
g
number of events
30
20
10
0
***
***
***
*
Retraction
No Retraction
Overlapping
Control
siRNA 1
siRNA 2
N-Cad
h
displacement
6
4
2
0
-2
-4
-6
***
ns
Control
siRNA N-Cad
Free Moving
Contact
Free Moving
Contact

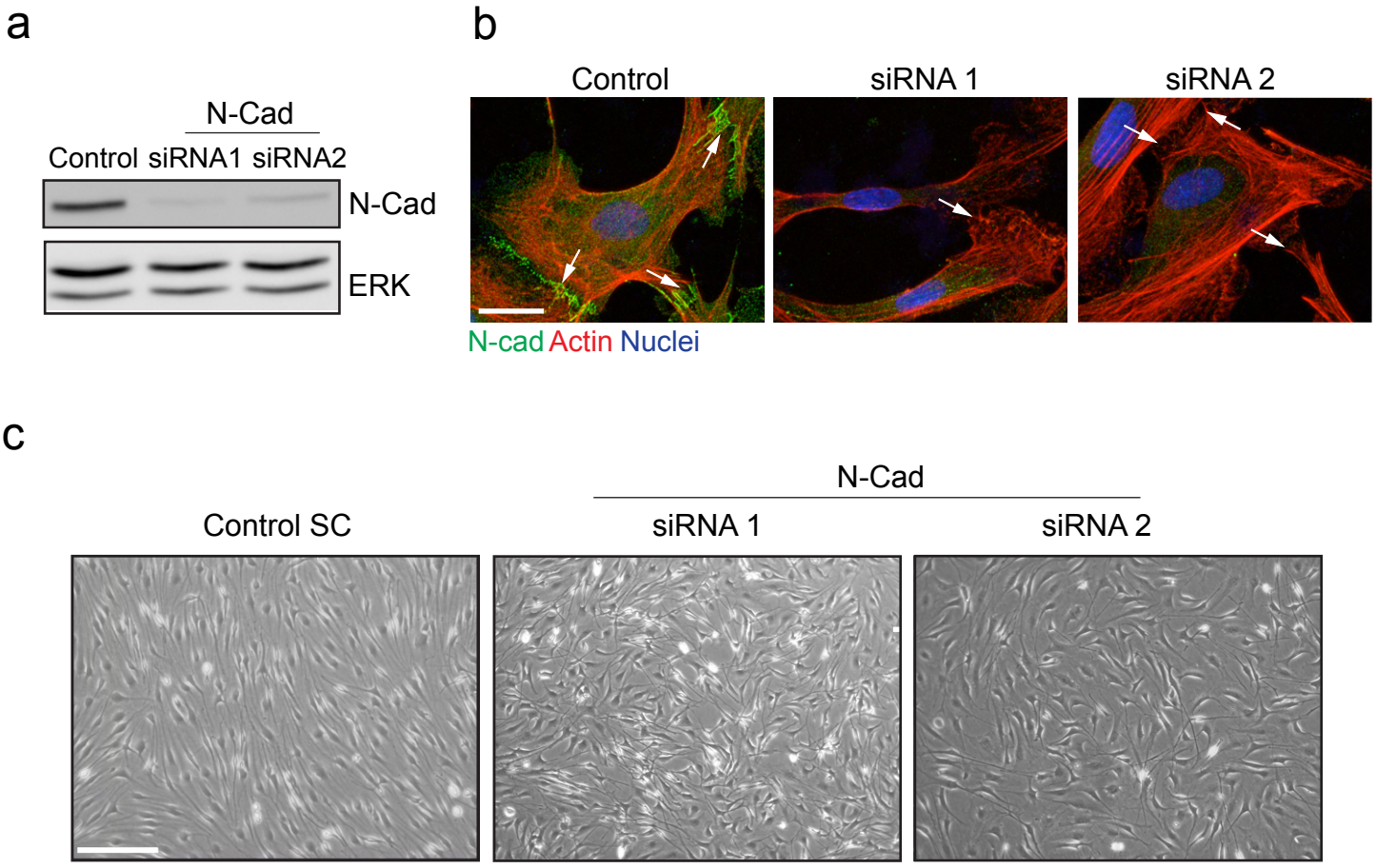
a
N-Cad
Control siRNA1 siRNA2
N-Cad
ERK
b
Control
siRNA 1
siRNA 2
N-cad Actin Nuclei
c
N-Cad
Control SC
siRNA 1
siRNA 2

Figure 2.

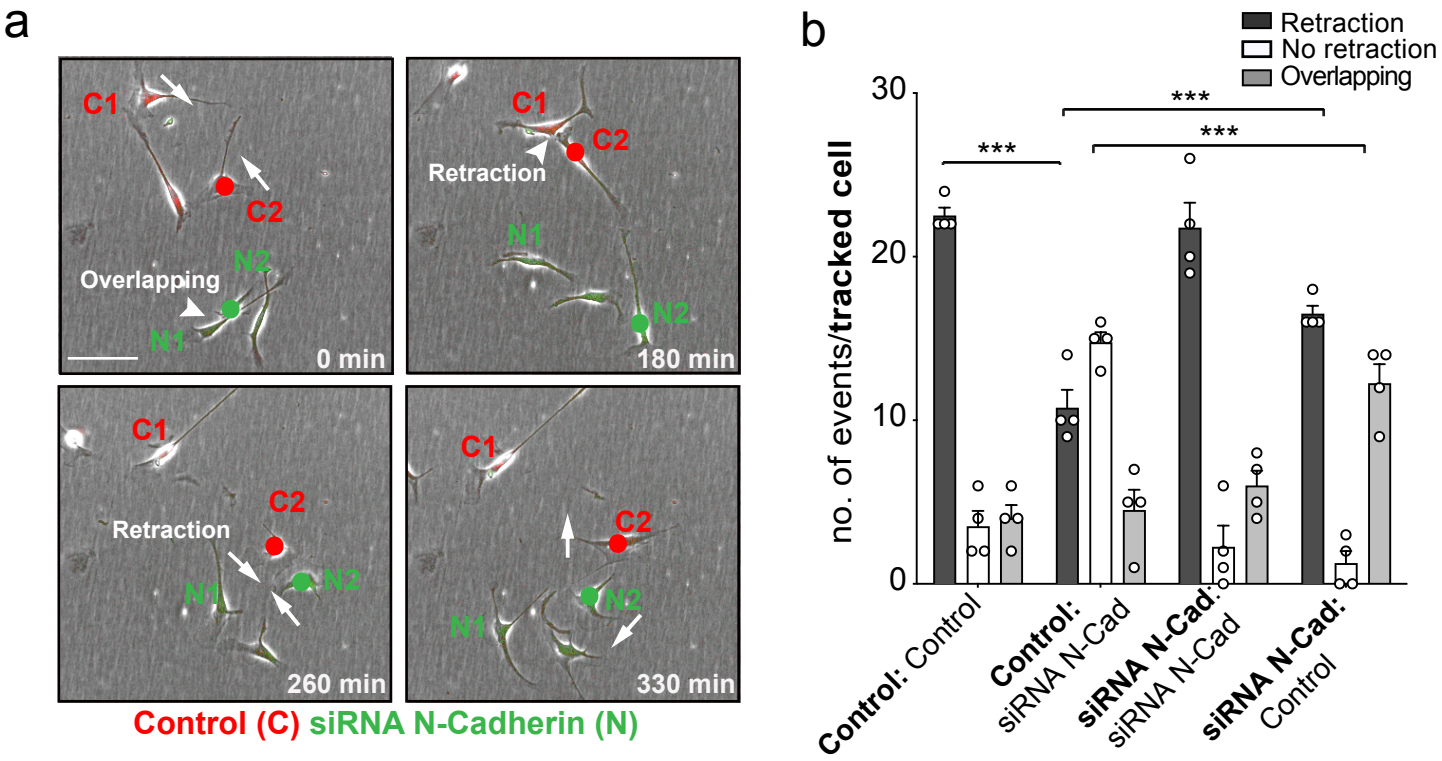
a
C1
C2
N1
N2
Overlapping
0 min
Retraction
180 min
260 min
330 min
Control (C) siRNA N-Cadherin (N)
b
Retraction
No retraction
Overlapping
no. of events/tracked cell
***
Control: Control
Control: siRNA N-Cad
siRNA N-Cad: siRNA N-Cad
siRNA N-Cad: Control

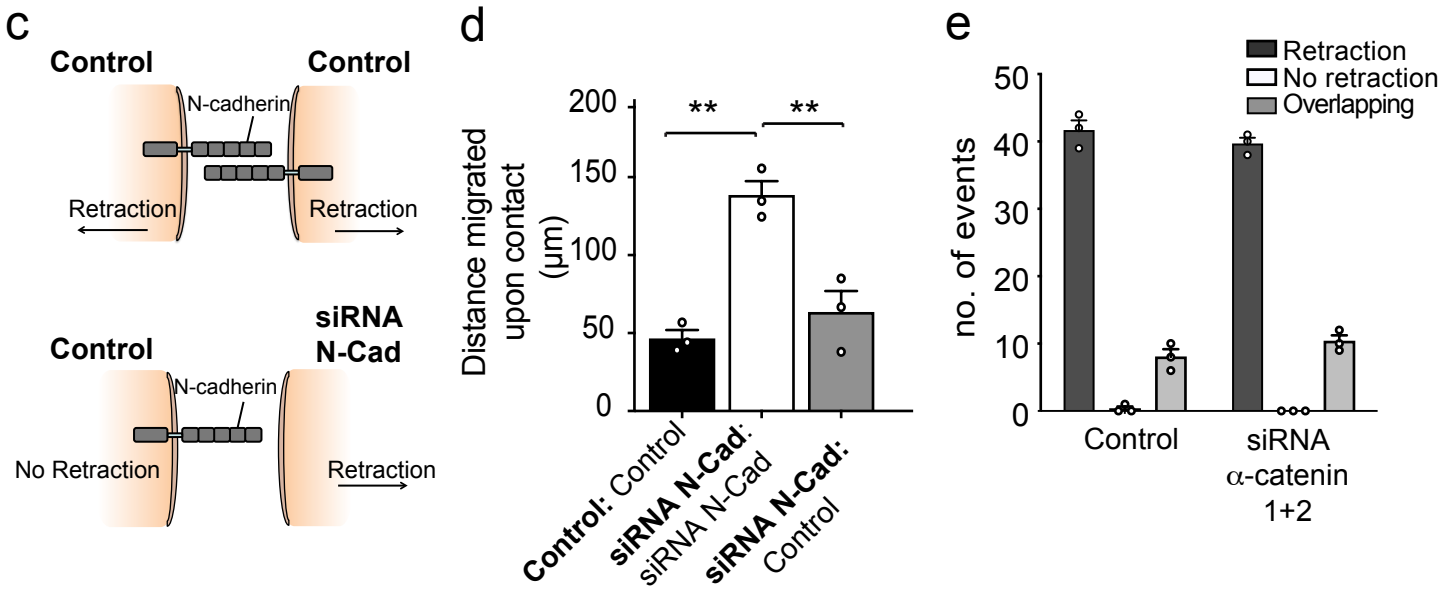
c
Control
Control
N-cadherin
Retraction
Retraction
siRNA N-Cad
Control
N-cadherin
No Retraction
Retraction
d
Distance migrated upon contact (µm)
**
**
Control: Control
siRNA N-Cad: siRNA N-Cad
siRNA N-Cad: Control
e
Retraction
No retraction
Overlapping
no. of events
Control
siRNA α-catenin 1+2

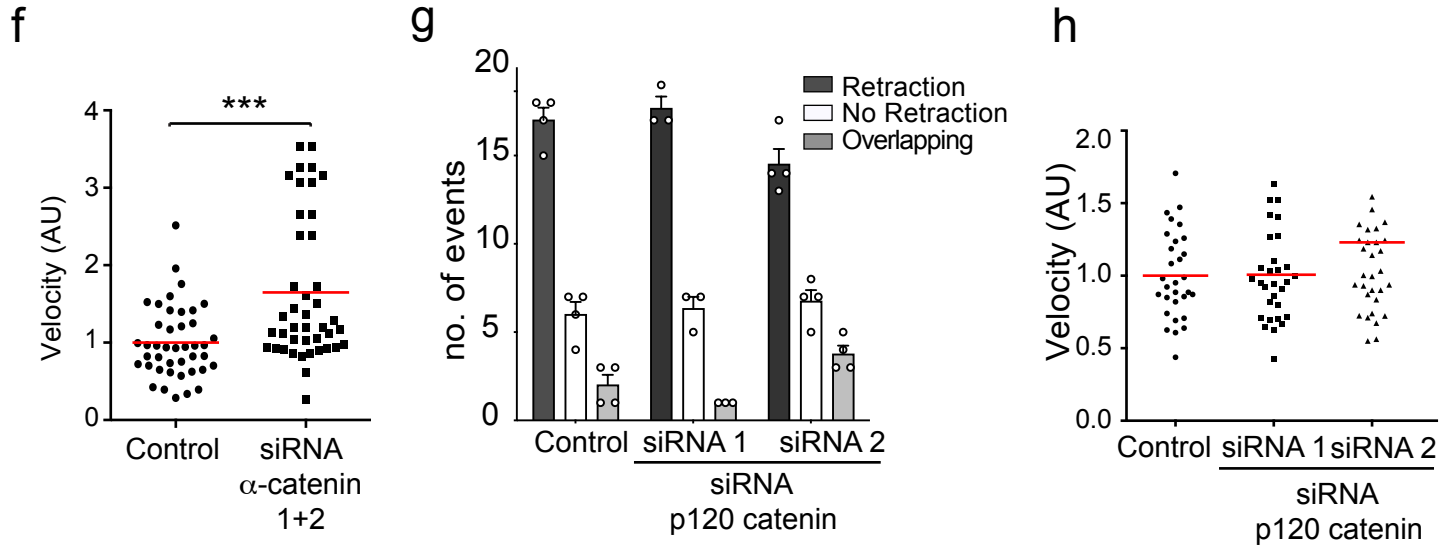
f
***
Velocity (AU)
Control
siRNA α-catenin 1+2
g
Retraction
No Retraction
Overlapping
no. of events
Control
siRNA 1
siRNA 2
siRNA p120 catenin
h
Velocity (AU)
Control
siRNA 1
siRNA 2
siRNA p120 catenin

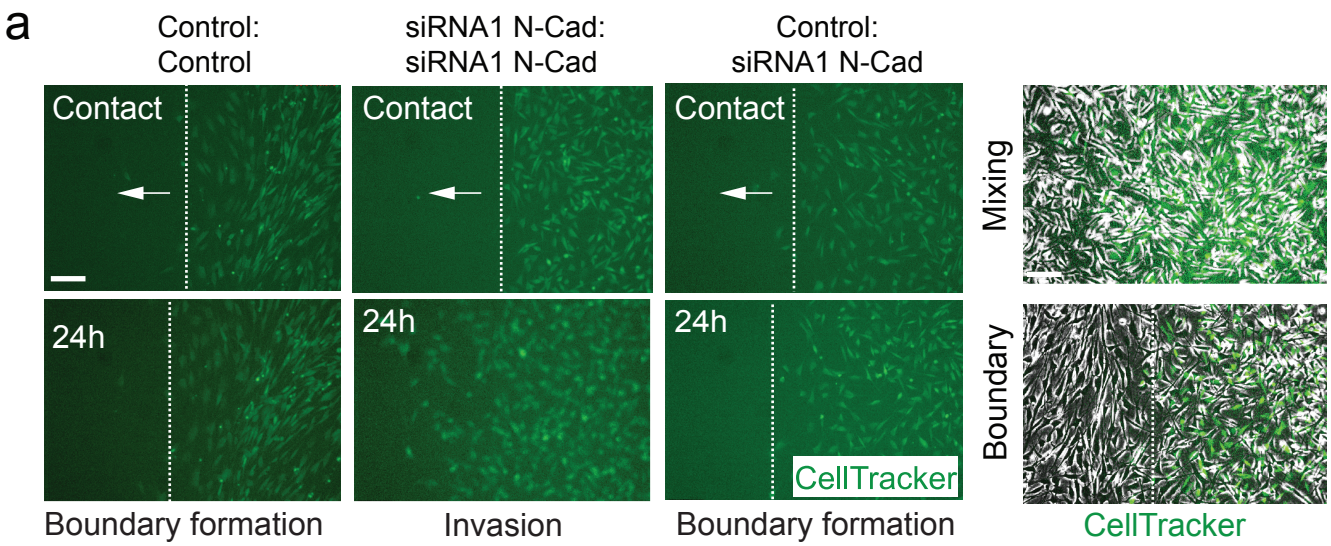
a
Control:
Control
siRNA1 N-Cad:
siRNA1 N-Cad
Control:
siRNA1 N-Cad
Contact
Contact
Contact
24h
24h
24h
CellTracker
Mixing
Boundary
Boundary formation
Invasion
Boundary formation
CellTracker

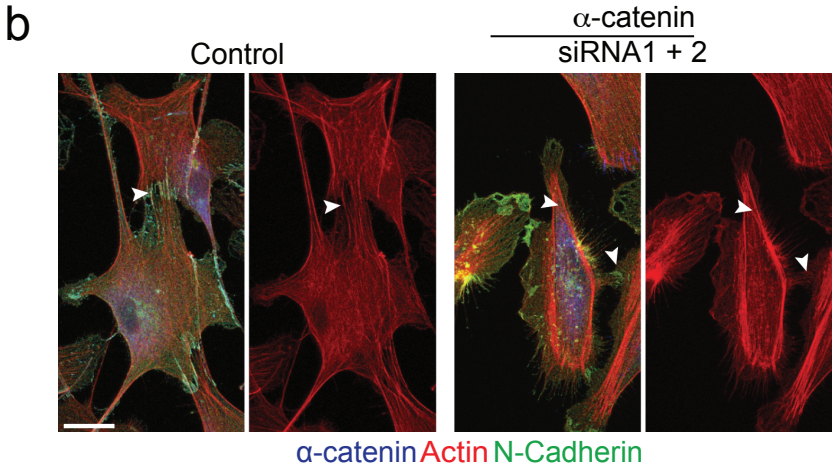
b
Control
α-catenin
siRNA1 + 2
α-catenin Actin N-Cadherin


c
siRNA
α-catenin
Control si1 si2 si1+2
α-catenin
ERK

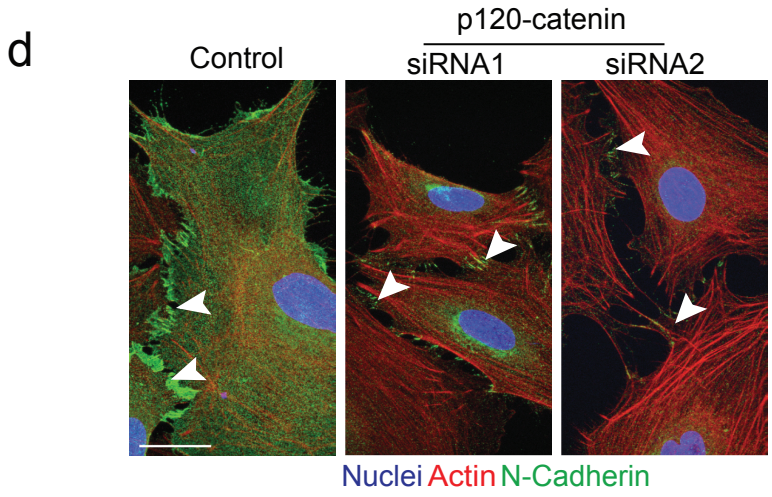
d
Control
p120-catenin
siRNA1
siRNA2
Nuclei Actin N-Cadherin

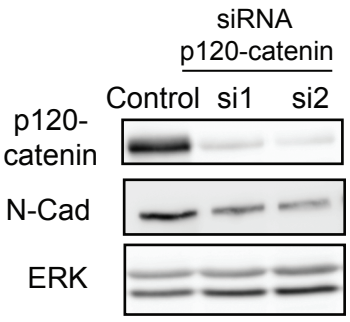
e
siRNA
p120-catenin
Control si1 si2
p120-
catenin
N-Cad
ERK

Figure 3.

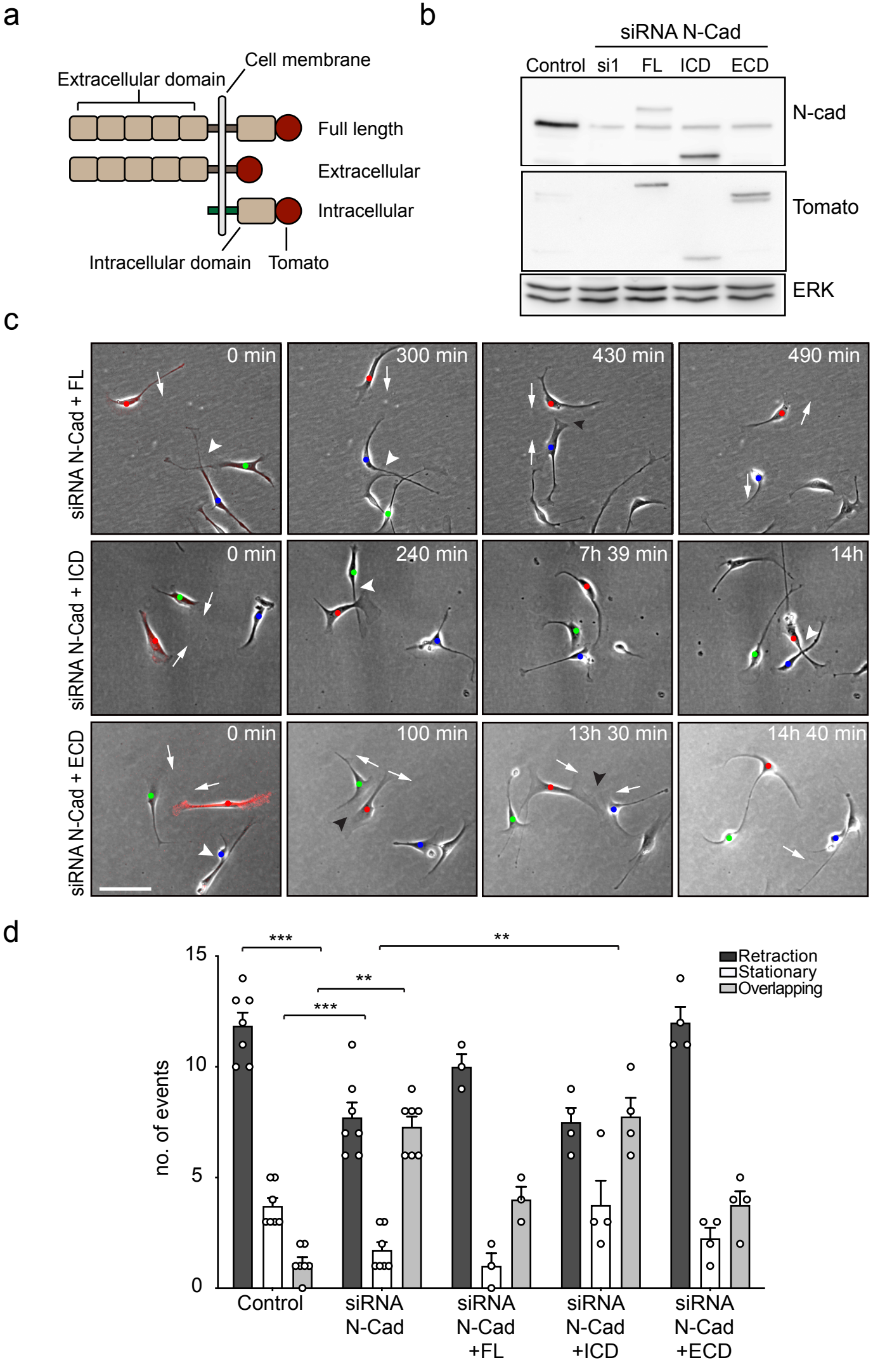
a
Extracellular domain
Cell membrane
Full length
Extracellular
Intracellular
Intracellular domain
Tomato
b
siRNA N-Cad
Control
si1
FL
ICD
ECD
N-cad
Tomato
ERK
c
siRNA N-Cad + FL
0 min
300 min
430 min
490 min
siRNA N-Cad + ICD
0 min
240 min
7h 39 min
14h
siRNA N-Cad + ECD
0 min
100 min
13h 30 min
14h 40 min
d
no. of events
15
10
5
0
***
**
***
**
Retraction
Stationary
Overlapping
Control
siRNA N-Cad
siRNA N-Cad +FL
siRNA N-Cad +ICD
siRNA N-Cad +ECD

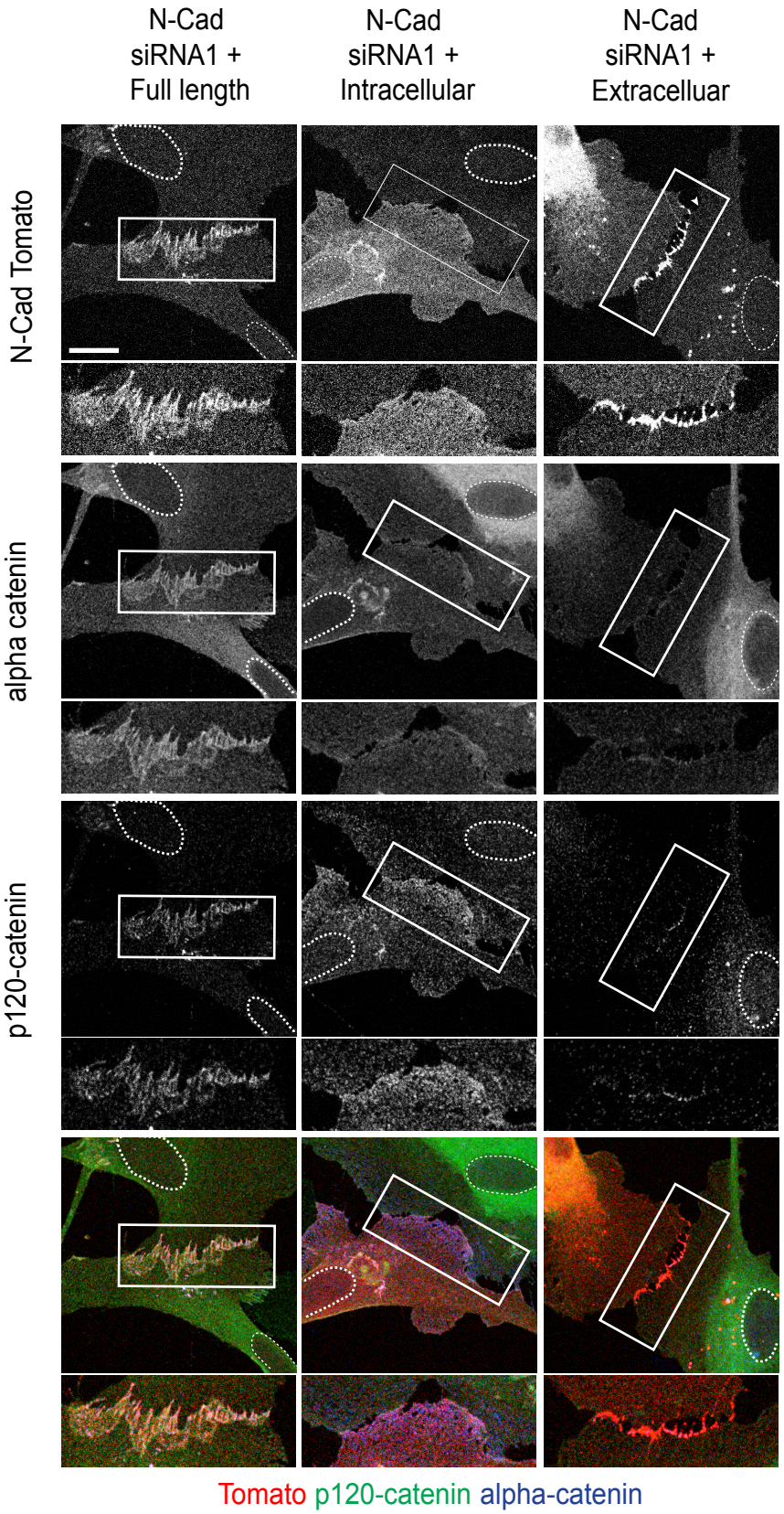
N-Cad siRNA1 + Full length
N-Cad siRNA1 + Intracellular
N-Cad siRNA1 + Extracelluar
N-Cad Tomato
alpha catenin
p120-catenin
Tomato p120-catenin alpha-catenin

Figure 4.

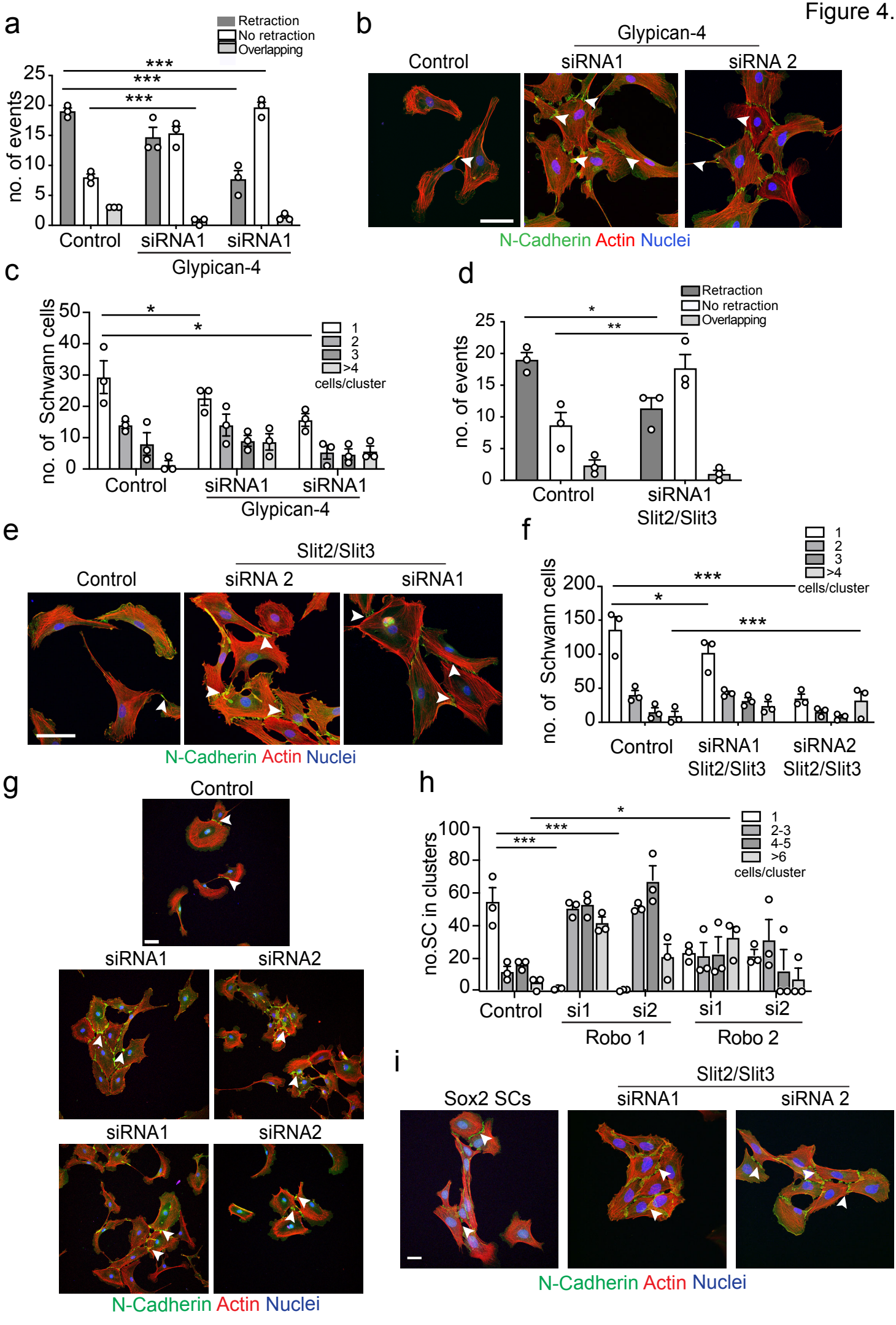
a
Retraction
No retraction
Overlapping
no. of events
Control
siRNA1
siRNA1
Glypican-4
b
Glypican-4
Control
siRNA1
siRNA 2
N-Cadherin Actin Nuclei
c
no. of Schwann cells
1
2
3
>4
cells/cluster
Control
siRNA1
siRNA1
Glypican-4
d
Retraction
No retraction
Overlapping
no. of events
Control
siRNA1
Slit2/Slit3
e
Slit2/Slit3
Control
siRNA 2
siRNA1
N-Cadherin Actin Nuclei
f
no. of Schwann cells
1
2
3
>4
cells/cluster
Control
siRNA1
Slit2/Slit3
siRNA2
Slit2/Slit3
g
Control
siRNA1
siRNA2
siRNA1
siRNA2
N-Cadherin Actin Nuclei
h
no.SC in clusters
1
2-3
4-5
>6
cells/cluster
Control
si1
si2
si1
si2
Robo 1
Robo 2
i
Slit2/Slit3
Sox2 SCs
siRNA1
siRNA 2
N-Cadherin Actin Nuclei

Supplementary Figure 4

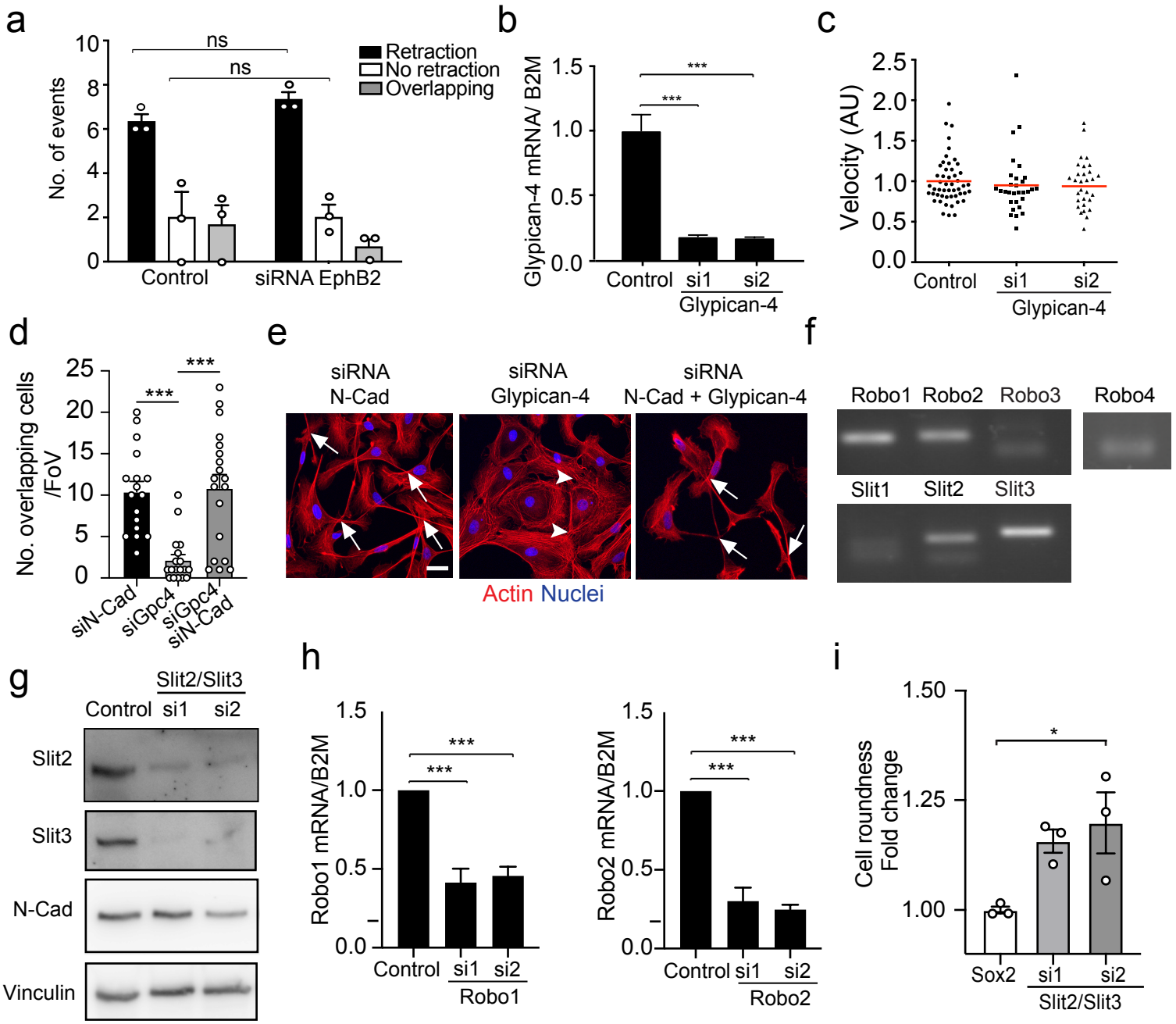

Figure 5.

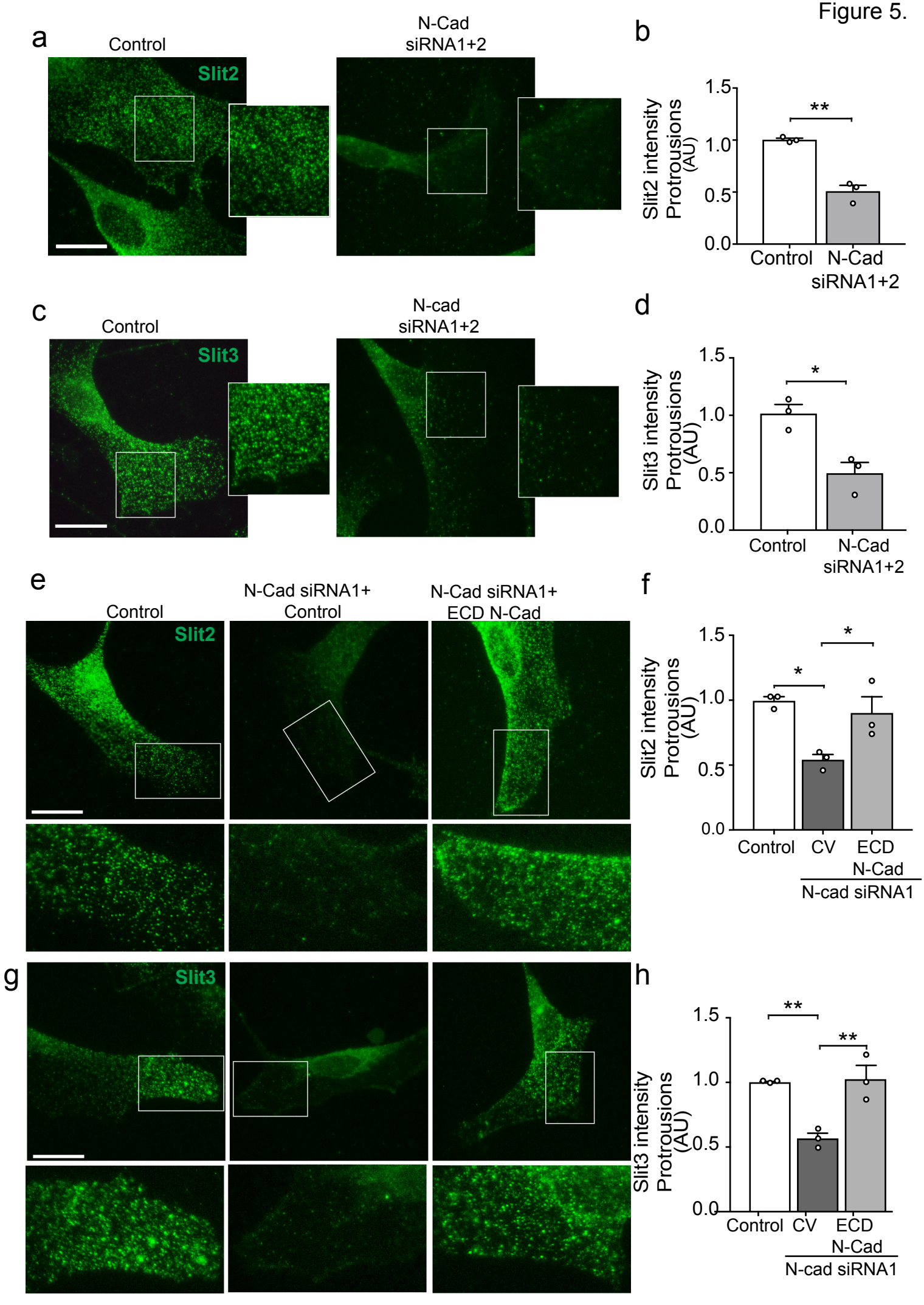
a
Control
N-Cad siRNA1+2
Slit2
b
Slit2 intensity Protrousions (AU)
1.5
1.0
0.5
0.0
**
Control
N-Cad siRNA1+2
c
Control
N-cad siRNA1+2
Slit3
d
Slit3 intensity Protrousions (AU)
1.5
1.0
0.5
0.0
*
Control
N-Cad siRNA1+2
e
Control
N-Cad siRNA1+ Control
N-Cad siRNA1+ ECD N-Cad
Slit2
f
Slit2 intensity Protrousions (AU)
1.5
1.0
0.5
0.0
*
*
Control
CV
ECD N-Cad
N-cad siRNA1
g
Slit3
h
Slit3 intensity Protrousions (AU)
1.5
1.0
0.5
0.0
**
**
Control
CV
ECD N-Cad
N-cad siRNA1

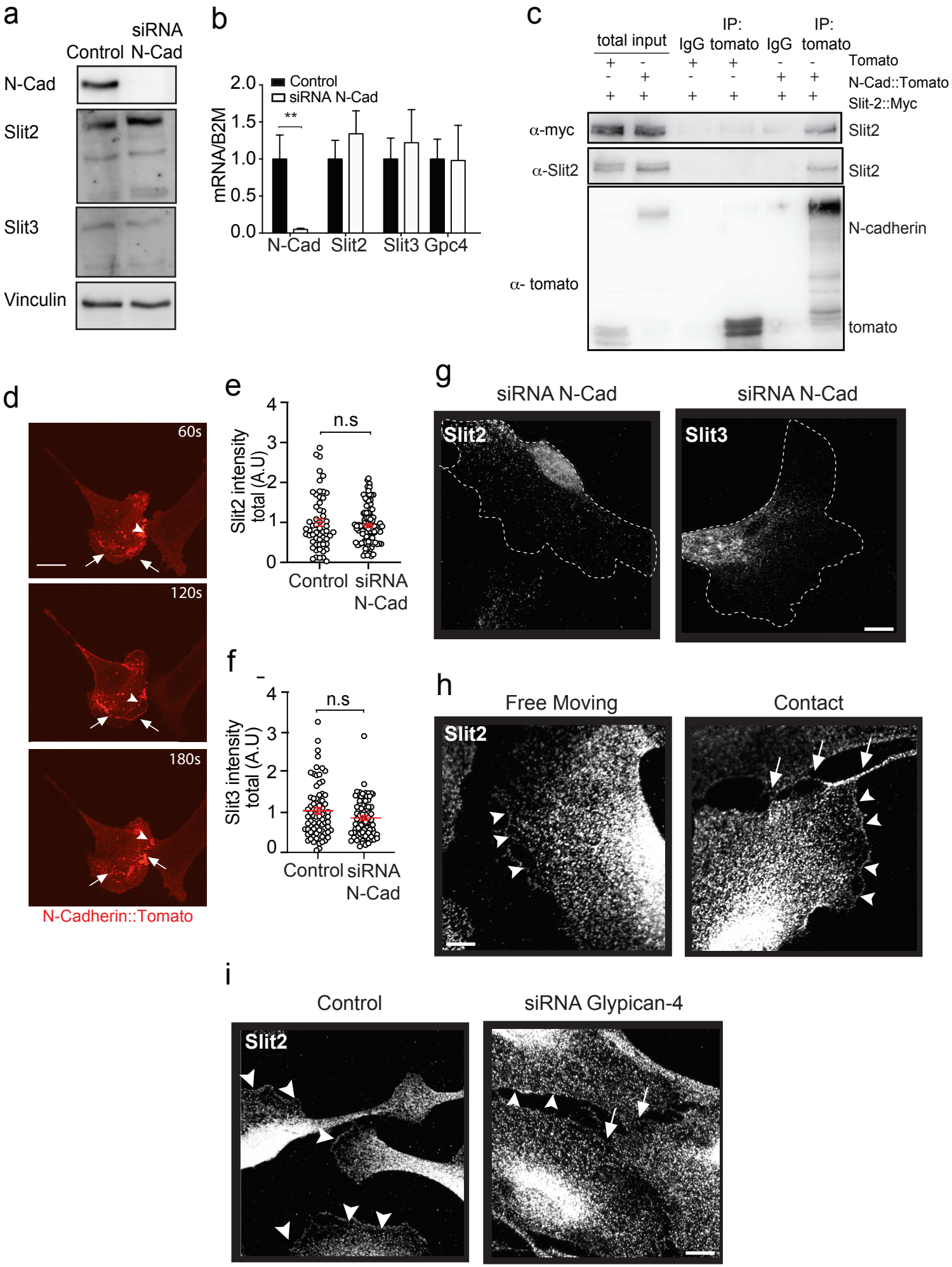
a
Control
siRNA N-Cad
N-Cad
Slit2
Slit3
Vinculin
b
Control
siRNA N-Cad
**
mRNA/B2M
2.0
1.5
1.0
0.5
0.0
N-Cad
Slit2
Slit3
Gpc4
c
total input
IP: IgG
IP: tomato
IgG
IP: tomato
Tomato
N-Cad::Tomato
Slit-2::Myc
α-myc
Slit2
α-Slit2
Slit2
N-cadherin
α- tomato
tomato
d
60s
120s
180s
N-Cadherin::Tomato
e
n.s
Slit2 intensity total (A.U)
Control
siRNA N-Cad
f
n.s
Slit3 intensity total (A.U)
Control
siRNA N-Cad
g
siRNA N-Cad
siRNA N-Cad
Slit2
Slit3
h
Free Moving
Contact
Slit2
i
Control
siRNA Glypican-4
Slit2

Figure 6.

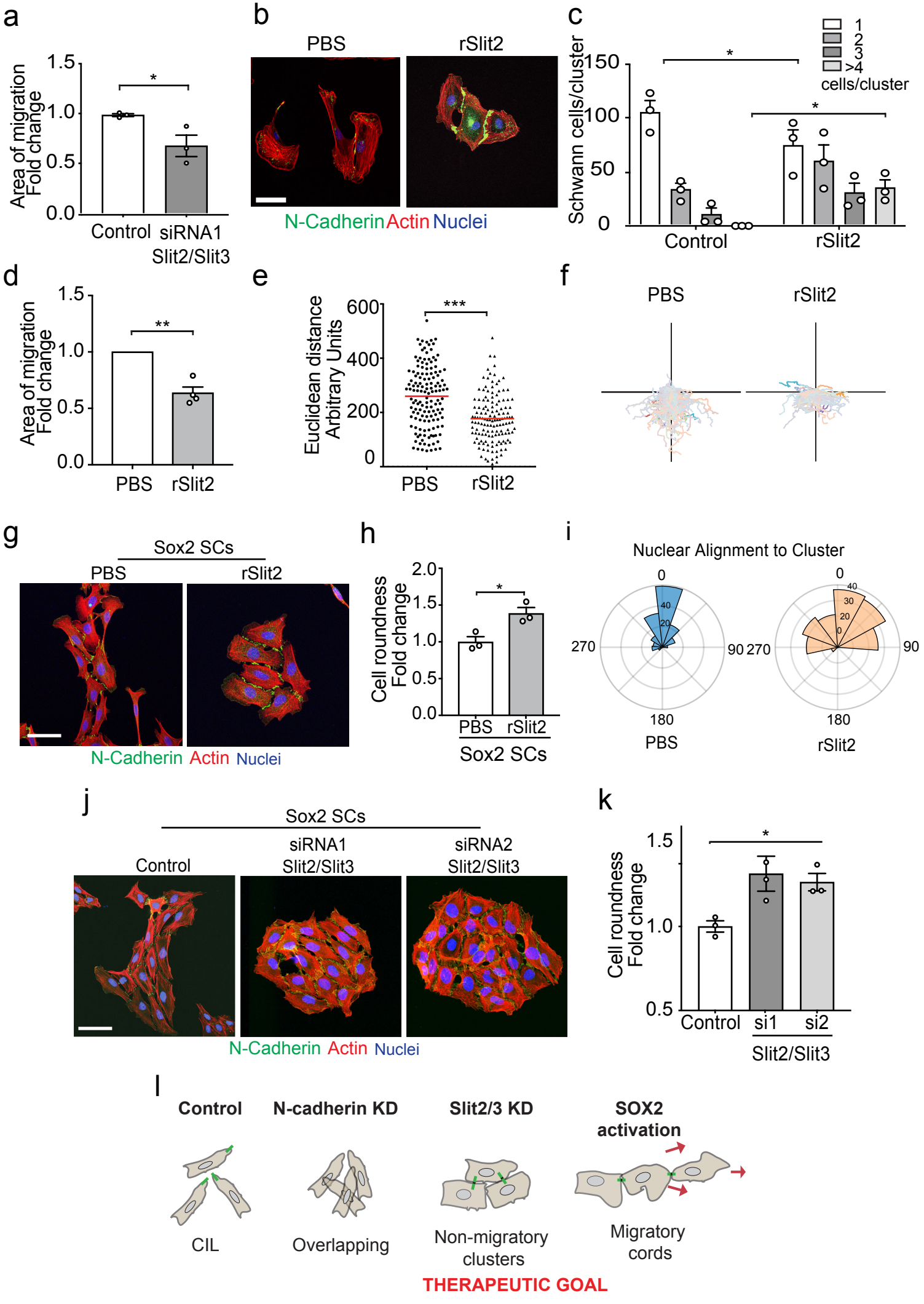
a
Area of migration Fold change
1.5
1.0
0.5
0.0
*
Control
siRNA1 Slit2/Slit3
b
PBS
rSlit2
N-Cadherin Actin Nuclei
c
Schwann cells/cluster
150
100
50
0
*
*
1
2
3
>4
cells/cluster
Control
rSlit2
d
Area of migration Fold change
1.5
1.0
0.5
0.0
**
PBS
rSlit2
e
Euclidean distance Arbitrary Units
600
400
200
0
***
PBS
rSlit2
f
PBS
rSlit2
g
Sox2 SCs
PBS
rSlit2
N-Cadherin Actin Nuclei
h
Cell roundness Fold change
2.0
1.5
1.0
0.5
0.0
*
PBS
rSlit2
Sox2 SCs
i
Nuclear Alignment to Cluster
0
90
180
270
40
30
20
0
PBS
rSlit2
j
Sox2 SCs
Control
siRNA1 Slit2/Slit3
siRNA2 Slit2/Slit3
N-Cadherin Actin Nuclei
k
Cell roundness Fold change
1.5
1.0
0.5
*
Control
si1
si2
Slit2/Slit3
l
Control
N-cadherin KD
Slit2/3 KD
SOX2 activation
CIL
Overlapping
Non-migratory clusters
Migratory cords
THERAPEUTIC GOAL

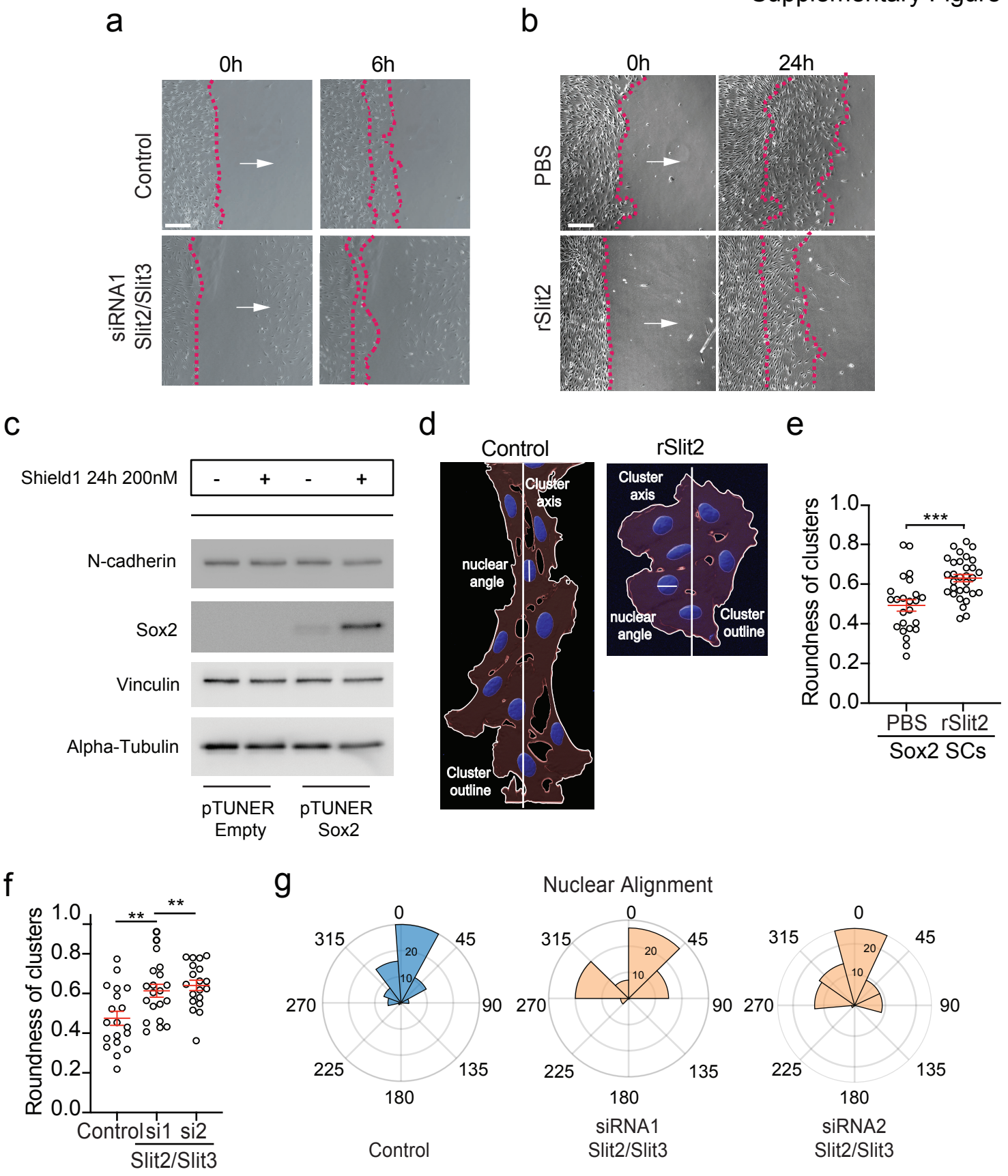
a
0h
6h
Control
siRNA1
Slit2/Slit3
b
0h
24h
PBS
rSlit2
c
Shield1 24h 200nM
- + - +
N-cadherin
Sox2
Vinculin
Alpha-Tubulin
pTUNER
Empty
pTUNER
Sox2
d
Control
rSlit2
Cluster
axis
nuclear
angle
Cluster
outline
e
Roundness of clusters
1.0
0.8
0.6
0.4
0.2
0.0
***
PBS
rSlit2
Sox2 SCs
f
Roundness of clusters
**
**
Control
si1
si2
Slit2/Slit3
g
Nuclear Alignment
0
45
90
135
180
225
270
315
20
10
Control
siRNA1
Slit2/Slit3
siRNA2
Slit2/Slit3

Figure 7.

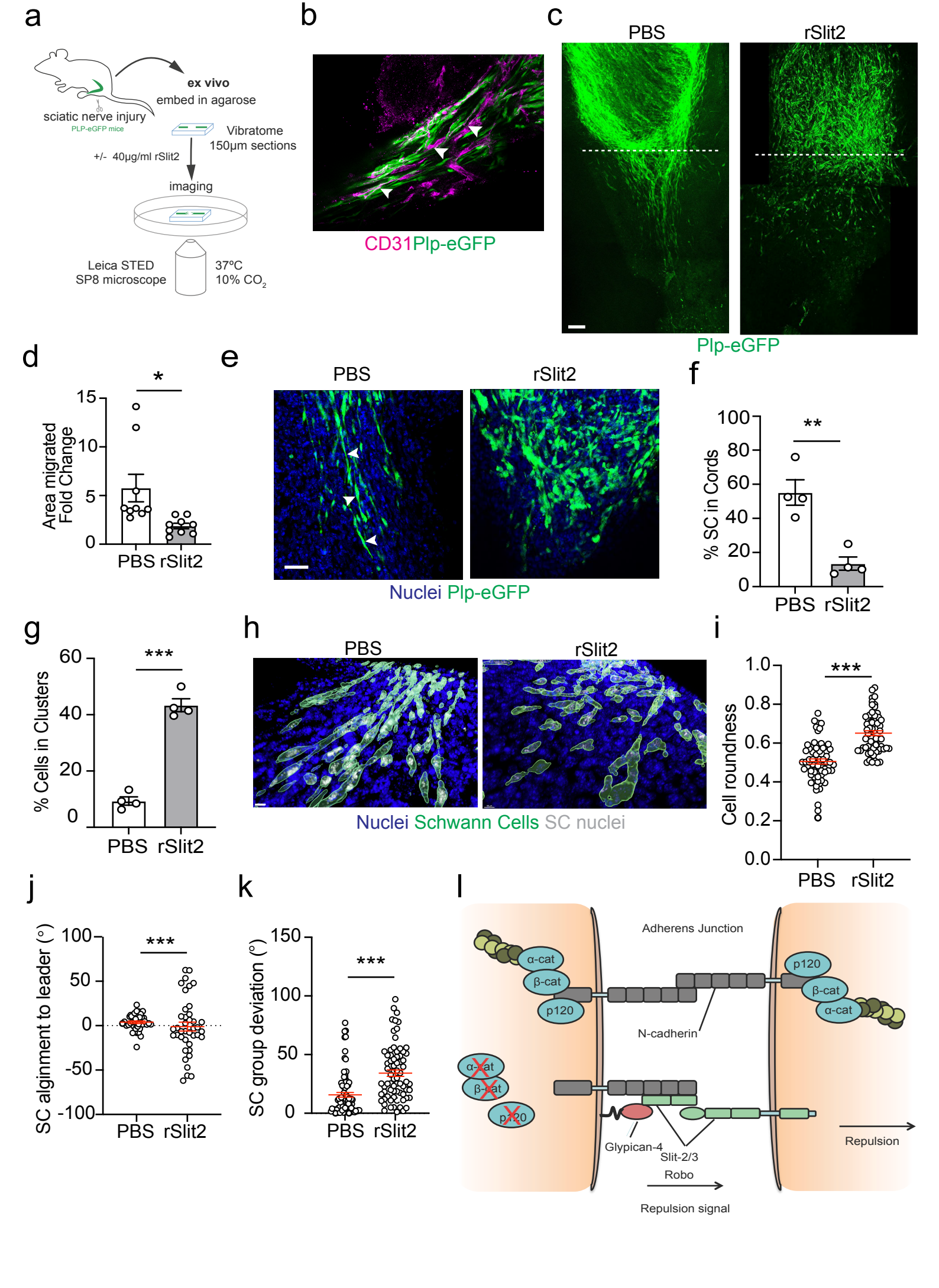
a
ex vivo
embed in agarose
sciatic nerve injury
PLP-eGFP mice
Vibratome
150µm sections
+/- 40µg/ml rSlit2
imaging
Leica STED
SP8 microscope
37ºC
10% CO2
b
CD31Plp-eGFP
c
PBS
rSlit2
Plp-eGFP
d
Area migrated
Fold Change
PBS rSlit2
e
PBS
rSlit2
Nuclei Plp-eGFP
f
% SC in Cords
PBS rSlit2
g
% Cells in Clusters
PBS rSlit2
h
PBS
rSlit2
Nuclei Schwann Cells SC nuclei
i
Cell roundness
PBS rSlit2
j
SC alginment to leader (°)
PBS rSlit2
k
SC group deviation (°)
PBS rSlit2
l
Adherens Junction
α-cat
β-cat
p120
N-cadherin
Glypican-4
Slit-2/3
Robo
Repulsion
Repulsion signal

a

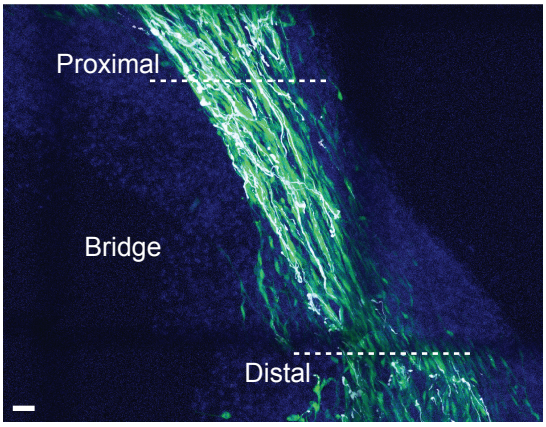

Plp-eGFP Axons Nuclei

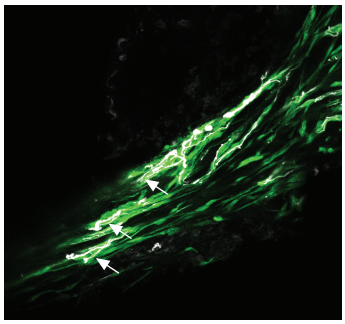

Plp-eGFP Axons Nuclei

b

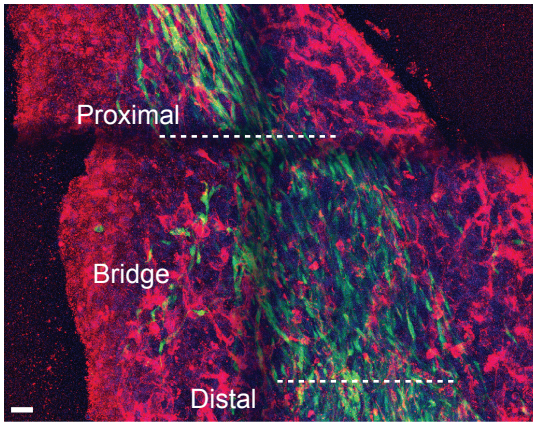

Plp-eGFP blood vessels Nuclei

c

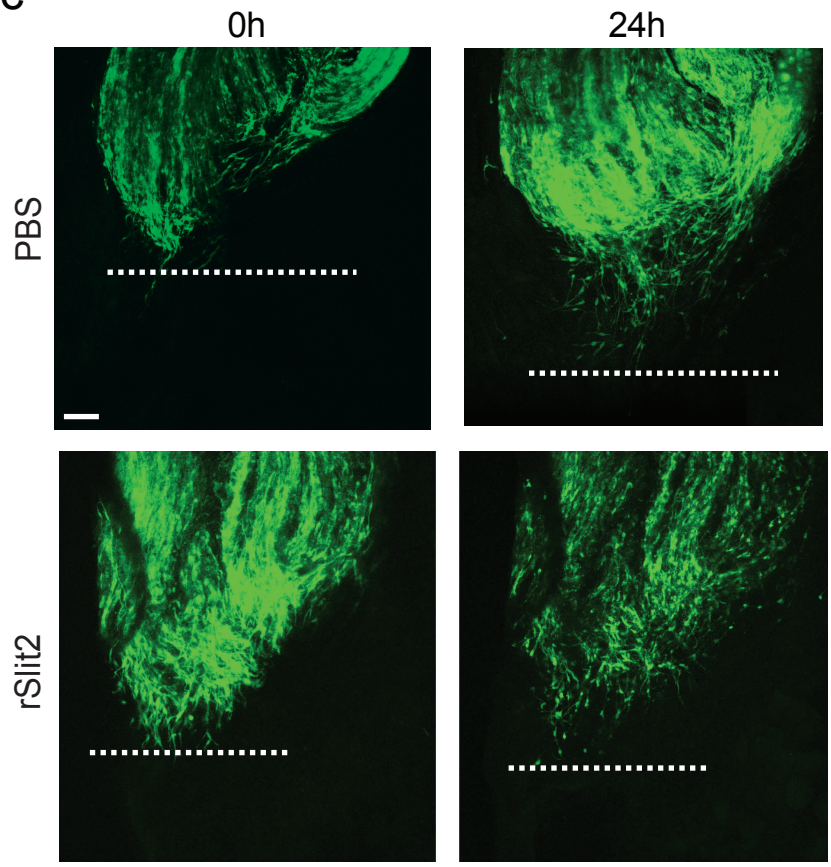

d

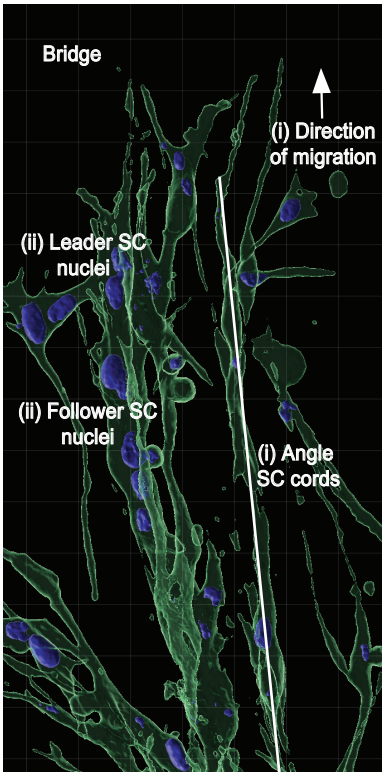

SCs Nuclei